Alma Mater Studiorum – University of Bologna

SCHOOL OF SCIENCE

Department of Industrial Chemistry "Toso Montanari"

Second cycle degree in

Low Carbon Technologies and Sustainable Chemistry

Classe LM-75 - Scienza e Tecnologie per l'Ambiente e il Territorio

Synthesis of antitumor modular conjugates for the preparation of nanocarriers with high affinity for endogenous albumin

Experimental degree thesis

CANDIDATE

Sofia Leo

SUPERVISOR

Prof. Mariafrancesca Fochi

CO-SUPERVISOR

Dott. Greta Varchi

Dott. Cecilia Martini

Academic Year 2020-2021

Index

ABSTRACT

Research on novel and more effective anticancer treatments has increasingly developed in the last decades. Among carcinomas, breast cancer has the highest incidence among women and its impact is steadily growing. According to the WHO, in 2020 there were 2.3 million women diagnosed with breast cancer and 685 000 deaths globally. As of the end of 2020, there were 7.8 million women alive who were diagnosed with breast cancer in the past 5 years, making it the world's most prevalent cancer.

Among breast cancers subtypes, triple negative breast cancer (TNBC) still lacks targeted and effective treatments options. Accounting for approximately 15–20% of all breast carcinomas, TNBC is associated with younger age of onset, aggressive clinical course, and dismal prognosis compared to hormone receptor and HER2-positive breast carcinomas. Despite the significant benefit provided by conventional chemotherapy and monoclonal antibodies in the prognosis of breast cancer patients, the treatment of this disease remains a great challenge.

Based on this, the aim of this work has been the development of a "*prodrug-based and bioresponsive approach*" to selectively target breast cancer cells. Through the setup of several synthetic procedures, we successfully designed and synthesized innovative paclitaxel (PTX) and epi-paclitaxel (epi-PTX) modular prodrugs capable of forming redox-sensitive nanoparticles able to specifically bind endogenous human serum albumin (HSA), to be selectively carried and released at the tumour site.

1. Introduction

1.1 - Brief historical notes on breast cancer

Cancer is the second leading cause of death in the world affecting humanity from prehistorical times. During the decades, the increase of environmental carcinogens, as well as of consumer products and the increasing risky health behaviours had led to new/modified cancer forms, that constantly hamper treatments efficacy and patients' recovery.

Nonetheless, the history of breast cancer has more deep foundations. It was the year 1200 B.C., time of the Trojan war, when Omero described on its opera the heroic performances of the Trojan and Greek army and the interventions of the gods in the war. The outbreak hitting humans and animals was attributed to the wrath of Apollo, but this believe did not convince Hippocrates.

The Hippocratic medicine was based on an accurate observation of the patient and his surroundings. In one of his characteristic short case-histories on breast cancer (BC), he described: 'A woman of Abdera had a carcinoma of the breast and there was a bloody discharge from the nipple. When the discharge was brought to a stand-still she died' (Hippocrates: Cinqieme livre des epidemies, 101). Hippocrates was aware of *καρκίνος or καρκίνωμα* (karkinos or karkinoma, cancer) of the nose, the uterus, the breast and the neck. He associated the origin of BC with the end of menstruation. Suppression of menstrual discharge would lead to engorgement of the breast and the appearance of nodules which would become increasingly indurated and ultimately degenerate into 'hidden' cancer. He probably used the term 'hidden' cancer to mean tumours which had not yet penetrated the skin. With regard the efficacy of medical treatment, Hippocrates was extremely reticent: 'It is better to give no treatment in cases of hidden cancer; treatment causes speedy death, and omitting treatment prolong women' life' [1]. In fact, the most common custom was to pray god Asclepius to offer relief from breast maladies, using as votive offerings with the shape of breasts.

The first trial of surgical intervention was considered as barbaric, especially by the Christian community, that preferred to wait a divine intervention, instead of using the surgical practice. Between the 16th and the 18th centuries, the medicine developed thanks to the anatomical exploration of human body, and for this reason new theories and therapies were developed for the treatment of breast cancer. In the 19th, also called the Golden Age of surgery, the situation completely changed thanks to new discoveries that made surgery safer and easier both for the patient and the surgeon [2]. Specifically, the use of sterile gloves and the process of disinfection and environment sterilization before the operation greatly improved surgical procedures. However, the most striking progress was brought by the introduction of anaesthesia that revolutionised completely the surgery's

world. The 19th and 20th centuries were characterised by big surgical interventions as well as the introduction of new BC therapies, as chemotherapy, radiotherapy, and several prevention campaigns were promoted, so that radical mastectomy could be avoided in some cases [2].

1.2 - Breast Cancer and Triple Negative Breast Cancer

Despite the enormous progresses made in BC prevention and treatment its impact has steadily increased in the last decades. As declared by the World Health Organization – WHO - in 2020 there were 2.3 million women diagnosed with breast cancer and 685 000 deaths globally. As of the end of 2020, there were 7.8 million women alive who were diagnosed with breast cancer in the past 5 years, making it the world's most prevalent cancer. BC subtypes are defined based on the immunohistochemical expression of estrogen and progesterone receptors, and HER2 overexpression or amplification. The three major BC subtypes are the hormone receptor (HR) positive, the HER2-enriched and the triple negative subtype (TNCB). This differentiation is crucial to implement more precise treatments for BC, validate tumor heterogeneity and treat these subtypes as completely distinct entities. TNBC accounts for 15-20% of all breast cancers (*Figure 1.2.1*). It lacks the expression of hormone receptors (ER/PR) while overexpressing the human epidermal growth factor (HER2).

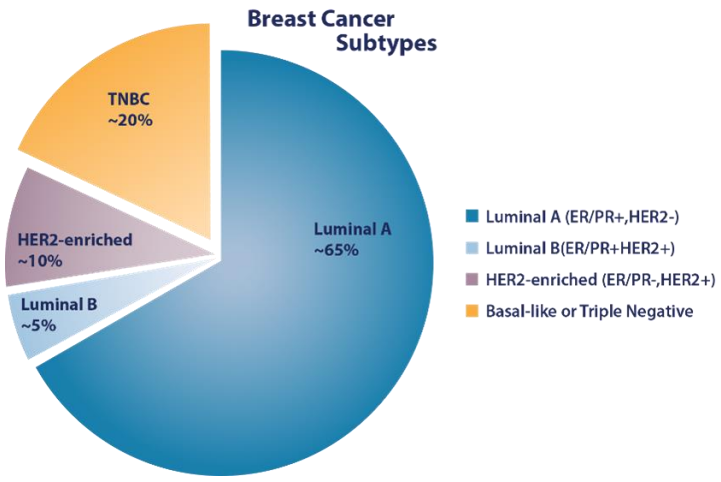

Figure 1.2.1 Pie chart of breast cancer subtypes (Abbviescience)

TNBC occurs with higher incidence in younger premenopausal women and is prevalent among African American descendants. It usually appears in the form of high-grade invasive ductal carcinoma and has a greater rate of early recurrences, often with distant metastases, and poorer prognosis compared to other BC subtypes. The evolution of the endocrine therapy for hormone receptor positive disease and anti-HER2 targeted treatment for HER2 amplified tumors, have resulted in significant improvement of prognoses for these patients. Unfortunately, despite the progress made

to elucidate tumor biology, clinical outcomes for TNBC remain unsatisfactory. The median overall survival for metastatic patients is approximately 18 months, much lower compared to the HR positive and HER2 enriched disease where survival may exceed five years. This fact emphasizes the compelling need to develop more effective treatments for TNBC patients [3].

1.3 - The birth of medical oncology

At the beginning of 1960s, medical oncology did not exist yet. During this period, scientists and few clinicians made the first studies on anticancer drugs. However, the entire medical community hampered these preliminary therapeutic approaches, affirming that the degree of systemic toxicity provoked by those drugs were not worthy. In 1974, thanks to the success of the first study on leukaemia, a protocol for treating cancer patients was slowly assessed and several institutions cooperated to implement it. A breakthrough happened for leukaemia and Hodgkin's disease, with the discovery of the activity of the alkaloids contained in the plant *Vinca rosea* and the properties of ibenzmethyzin (procarbazine) [4]. It was discovered that to completely eradicate cancer cells it was necessary to also eliminate all residual cancer cells; based on this, Jacob Furth and Morton J. Kahn proposed the "Cell Kill" hypothesis: a certain drug dosage will kill a constant percentage of cells rather than a constant number of cells. Repeated doses of chemotherapy were thus needed to reduce the total number of cells. At this moment, the idea of using a combination of drugs was first considered.

1.4 - The Adjuvant Chemotherapy

Thanks to the success of chemotherapy in the cure of advanced state tumors, scientists started thinking about using systemic chemotherapy at the earliest stage of the disease. Indeed, Dr. Howard Skipper hypothesized that if drugs were effective in the advanced disease stage, they could be even more effective at tumor presentation, e.g., adjuvant chemotherapy [4].

Two programs were designed to test the efficacy of this approach: one was the L-PAM (L-phenylalanine mustard) and the second was the CMF program, a combination of cyclophosphamide, methotrexate, and 5-fluoracil. Results from the CMF trial were astounding showing an overall response rate over 50%, with about 20% of patients in complete remission. Despite this success, not every surgeon was convinced in testing this kind of treatment. Only Dr. Bernard Fisher that had already tested the adjuvant chemotherapy with his group NSABP (National Surgical Adjuvant Breast Project), accepted the challenge. Unfortunately, anyone in the USA was prepared to use combination

chemotherapy for treating BC, and for this reason Dr. Francesco Bonadonna from the Istituto Nazionale Tumori of Milan agreed to perform the study [4]. He used a slightly dose-reduced version of CMF versus no therapy. The two studies were completed during the following five years and results of both were positive, therefore translating into a cascade of adjuvant studies for BC and other types of tumours.

1.5 - National Cancer Act

The successes achieved in the oncology field culminated in 1971 with the National Cancer Act. This event signed the beginning of modern oncology and opened the doors to a never-ending period of expansion and development of anticancer chemotherapy. New drugs were tested, new chemotherapy programs were expanded, and new testing model were developed. In 1975, the L1210 mouse model was abandoned in favour of human xenografts in nude mice. The goal of this research was to setup a more predictive model of anticancer drugs efficacy in humans. Taxanes, the molecules that will be discussed in this work, were identified as antitumour agents within this program. In parallel, the NCI panel of 60 human cancer cell lines was implemented allowing *in vitro* drugs optimization before the *in vivo* tests.

An important event that promoted the development of new molecular targets was the Special Virus Cancer Program (SVCP) in 1960s. It was conceived as a crash program to identify viruses that could be associated with cancer. In the end, it failed becoming the Program of Molecular Biology to study genes that were co-opted by tumour viruses. Thanks to this program, most of the compounds currently used for developing new anticancer drugs were identified, such as oncogenes, suppressor oncogenes, and signalling pathways essential for developmental biology. SVCP also helped in the genome sequencing and for the understanding that cancer abnormalities are often due to abnormal function of protein kinases, thus leading to new studies that are currently ongoing [4]. All these discoveries represent the pillars of modern medical oncology, which is increasingly focused on rationally combine novel targeted therapy with old drugs, with the final goal of making cancer curable.

2. Target cancer therapy

Targeted therapy mainly differs from classic chemotherapy by the mechanism of action. Targeted therapy interferes with specific proteins involved in tumorigenesis. It is possible to divide target cancer therapy in three types:

i. Monoclonal antibodies
ii. Small molecule inhibitors
iii. Immunotoxins

Monoclonal antibodies exert their anticancer effects through multiple mechanisms: activating the immune system, inhibiting the interactions between ligand and receptor, or transporting a lethal toxin (immunotoxins) to the cancer cell [5].

Small molecules inhibitors block specific enzymes and growth factors receptor. Much research is focusing on this field trying to develop new kind of molecules that can act as inhibitors. The most famous approved are the Gleevec (imatinib mesylate) to treat myelogenous leukaemia and the Iressa (geftinib) to treat non-small cell lung cancer.

Immunotoxins are proteins that contain an antibody with a toxin or growth factor that can specifically bind to target cells

2.1 – Paclitaxel: origin, mechanism of action and formulations

Paclitaxel (PTX) (***Figure 2.1.1 B***) is a secondary metabolite produced by *Taxus sp. (**Figure 2.1.2 A**),* and in smaller quantity by *Podocarpus gracilior, Corylus avellana.* It was in 1960s when paclitaxel was identified for the first time by Dr. Jonathan L. Hartwell from the bark of *Taxus brevifolia.* Its chemical structure was elucidated in 1971 and clinical trials began in 1984. However, major issues related to production costs from the tree together with environmental constraints, required the setup of alternative strategies for its production.

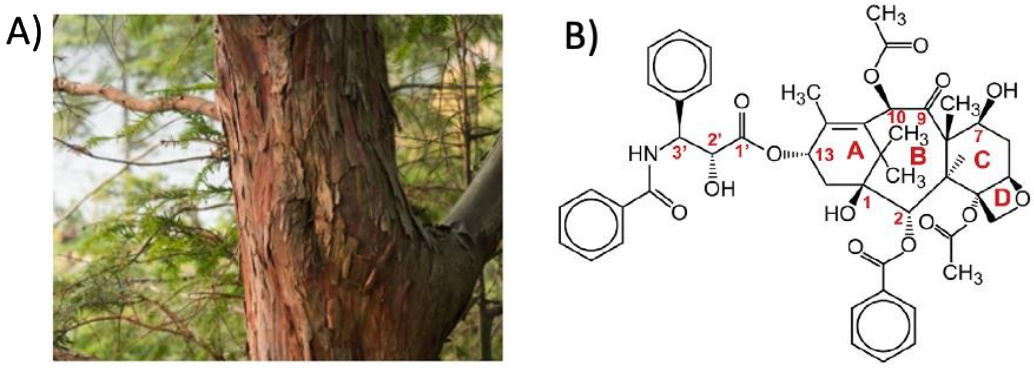

*Figure 2.1.2 A) Bark of Taxus brevifolia; **B)** Chemical structure of Paclitaxel*

In 1994, the pharmaceutical company Bristol-Myers Squibb successfully scaled-up a semisynthetic process for the synthesis of PTX, also known with the commercial name of Taxol®, starting from its precursor 10-deacetyl baccatin, which is found in the leaves of European Taxus.

In 1998, the American Food and Drug Administration (FDA) and the European Medicines Agency (EMA) approved the use of Taxol® for the treatment of breast, ovarian, lung cancer and Kaposi's sarcoma.

Paclitaxel *mechanism of action* includes the induction of cellular death through binding to tubulin and inhibiting the disassembly of microtubules. The production of the microtubule and tubulin occurs during the G2 phase of the cell cycle (when the cell is ready for the mitosis). Microtubule targeting agents (MTA) are divided into two categories: stabilizing agent, such as Taxol®, and destabilizing agent, as *Vinca alkaloids*, which bind to α/β tubulin and disassemble microtubules. The cells exposed to PTX are confined in the G2/M-phase leading to cell death. Furthermore, it was recently demonstrated that PTX produces an increase in ROS and an overexpression of proteins and genes caused by the endoplasmatic reticulum (ER) stress in osteosarcoma cells. This stress causes the release of Ca^{2+}, causing an overload and mitochondrial damage, and so an increase in ROS concentration [6].

Paclitaxel anti-cancer activity (**Fig. 2.1.2B**) is principally related to ring A, the oxetane D ring ring, the C2 benzoyl group, and other components, such as the C3' amide-acyl group and the OH group at C2' position of the side chain. Other groups (on the C9 carbonyl group and on the C10 the acetyl group) influence the therapeutic activity only slightly. However, the C10 acetyl group is important because it contributes to the characteristic conformation of the paclitaxel molecule. The OH groups at the C2' and C7 positions are the most suitable for prodrugs formation because their functionalization nullify PTX biological activity, while being relatively reactive to undergo semi-synthetic modifications [7].

In 2000, Taxol® global sales were around 1.5 billion dollars. However, the discovery of a safer nanotechnological PTX formulation based on albumin nanoparticles, e.g., Abraxane®, able to greatly reduce systemic toxicity and improve patient compliance, strongly shorten the clinical application of Taxol®[8]

Abraxane is obtained through the so called Nab-technology [9], including a high-pressure homogenization procedure which allow the formation of stable nanoparticles only under un-diluted conditions, while quickly disassembling once intravenously injected. Another critical challenge of the Abraxane formulation is represented by the limited drug loading [10]. During the last decades, several alternative approaches have been studied to improve PTX formulation and delivery, such as the use

of peptides, proteins, antibodies, and polymers. Most of them, including the one that I will be discussing in my work, are based on the use of prodrugs able to release the active ingredient upon specific internal stimuli (e.g., as acidic environment, elevated reactive-oxygen species (ROS) level, increased glutathione (GSH) level, etc.) that are typical of tumour tissues [6].

2.2 - The problem of drug delivery

Besides the intrinsic and non-selective toxicity of most anticancer drugs, another critical issue is often represented by their difficult in-water formulation. In fact, most of these molecules are poorly water soluble, thus requiring the use of toxic solvents and surfactants for an effective administration. Furthermore, the treatment efficacy depends significantly on the delivery method: an overdose would most probably be harmful to the patient, whereas a too low concentration wouldn't produce the desired effect. Avoidance of healthy tissues, thus reducing unwanted side effects, represents another important challenge [11].

The main reasons that hamper or complicate anticancer drugs administration and delivery are:

- Limited water solubility of the active ingredients that might range between 0.1 to 1 mg/mL for the slightly soluble compounds to < 0.1 mg/mL (100 µg/mL) for compounds basically water insoluble. Of note, most anticancer drugs (40% to 70%) falls within these two categories.
- Poor bioavailability obstacles have been encountered in the attempt to cure severe disease and this is caused often by the inadequate and variable inter- and intra-patient bioavailability of the administered drugs. This inconvenience too often translates into inefficient treatment and increased costs for the patient and so, greater risks of toxicity or even death.
- Introduction of new drugs for which it is not already clear how to deliver them in the body
- Harmful side effects
- Uncontrolled or poorly controlled delivery of the drug: the therapeutic outcome of a drug treatment can be optimized controlling the rate at which it is delivered over a given period of time and also the extent of its release into the body. The efficacy of a controlled release is undermined by the premature release and loses of highly toxic anti-tumor drugs, such as paclitaxel, before reaching the targeted site. To address this issue, many types of controlled release systems with smart stimuli-responsive nano-systems are currently investigated [11].

3. The Tumour Microenvironment (TME)

One major feature of cancer is its genomic instability, responsible for the insurgence of several and unpredictable mutations and alterations. These mechanisms might end up in the formation of tumour antigens, that are recognized by the system as strangers thus provoking cellular immune response [12]. For this reason, the comprehension of genomic alterations and crosstalk between tumor cells and its microenvironment (TME) is essential to design novel and effective targeted therapies.

The tumor microenvironment forms when cancer cells begin to invade and change the surrounding tissue architecture. TME is a complex ecosystem composed of tumor cells, immune cells, and stromal cells, which provides a protective niche for tumor cells to thrive. Common abiotic features of TME include low oxygen concentrations, altered metabolite accumulations, acidic pH, as well as a collection of immunosuppressive cytokines and growth factors (***Figure 3.1.1***). Considering the still unmet need of reducing cancer chemotherapy systemic toxicity, the distinctive features of TME represent a great opportunity for the design of selective and targeted cancer therapy.

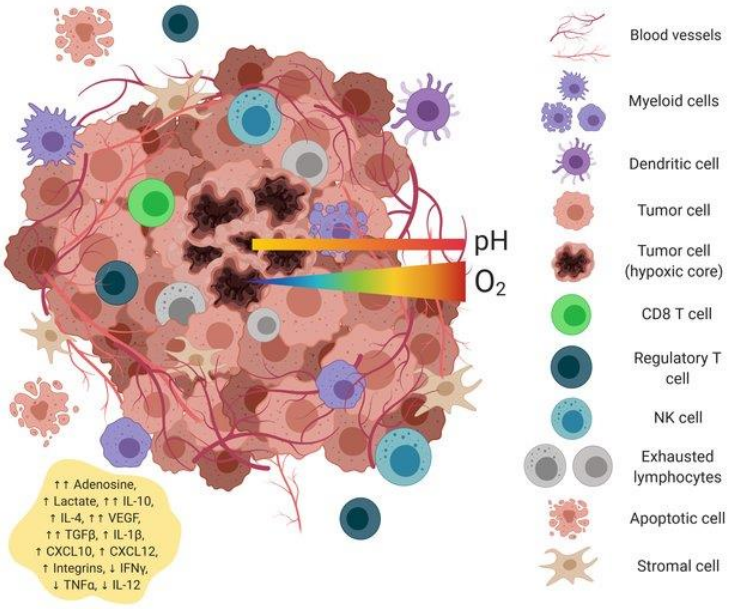

Figure 3.1.1 The architecture of tumor microenvironment [13]

Tumor cells grow very quickly and require elevated supply of nutrients from blood circulation. For this reason, they trigger the generation of new blood vessels in a process called angiogenesis. Due to their high growth rate, the newly formed blood vessels present fenestrations or leaky pores that allow to circulating agents, even the nano-sized ones, to leave the vasculature and “extravasate” into the tumor.

This “leaky” vasculature combined with the compromised lymphatic drainage within the tumor, represents the basis of the Enhanced Permeability Retention effect (EPR effect), which ultimately allow nanomedicines to preferentially enter and be retained into the tumor mass (**passive targeting**) [14] (**Figure 3.1.2**).

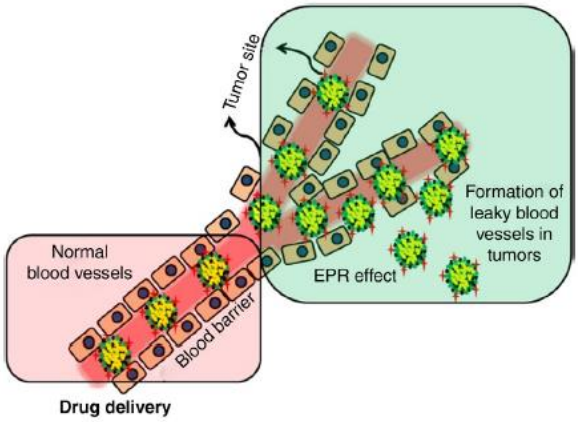

Figure 3.1.2 Schematic explanations of nanomaterials in tumor tissue by EPR effect, normal cells are lined by compact endothelial cells [15].

In general, the accumulation of nanoparticles in tumor tissues depends on several factors including their size, their surface features, their circulation half-life, and the degree of tumor angiogenesis.

The passive strategy is further limited because certain tumours do not exhibit the EPR effect, and the permeability of vessels may not be the same throughout a single tumour [16]. To increase the targeting effectiveness of nanoparticles, they can be modified with small ligands to increase the tumor selectivity. This targeting approach, that foresees the presence of receptor binding ligands on the nanoparticles surface, is known as **active targeting**, which allows the selective recognition of the nanoparticles from specific cells over-expressing those receptors.

In the present study, we focused our attention on the production of redox-responsive nanoparticles, containing disulfide bonds that are stable in the slightly oxidizing extracellular environment, but undergo thiol cleavage and disassembly in the presence intra-tumor reducing GSH.

3.2 - TME and drug delivery

A prodrug is an inactive form of a drug that that could be readily activated through a biocatalytic mechanism or through a spontaneous process (e.g. hydrolytic degradation), when reaching the pharmacological target thus allowing a selective selease of the drug.

The general structure of a prodrug is depicted in **Fig. 3.2.1**.:in blue the targeting moiety for specific delivery to the site of interest, such as polypeptides or monoclonal antibodies (mAb), in violet, the active moiety for anticancer activity (i.e. drug) and in black, the cleavable labile chemical moiety (i.e. linker) which is conjugated to the active moiety through a functional group.

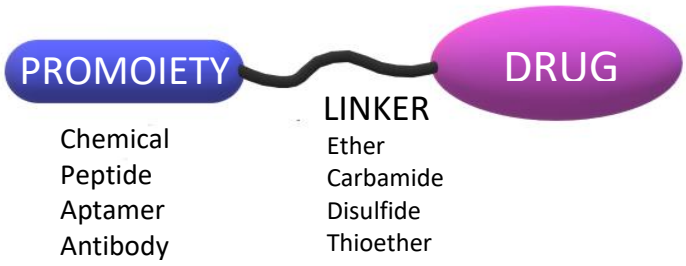

Figure 3.2.1 General structure of a prodrug

Tumor microenvironment (TME) is controlled and determined mainly by the reduction and oxidation states of Dihydronicotinamide-adenine dinucleotide phosphate (NADPH/NADP+) and glutathione, (GSH/GSSG), both of which have different reduction potentials and capacities (figure 3.2.2).

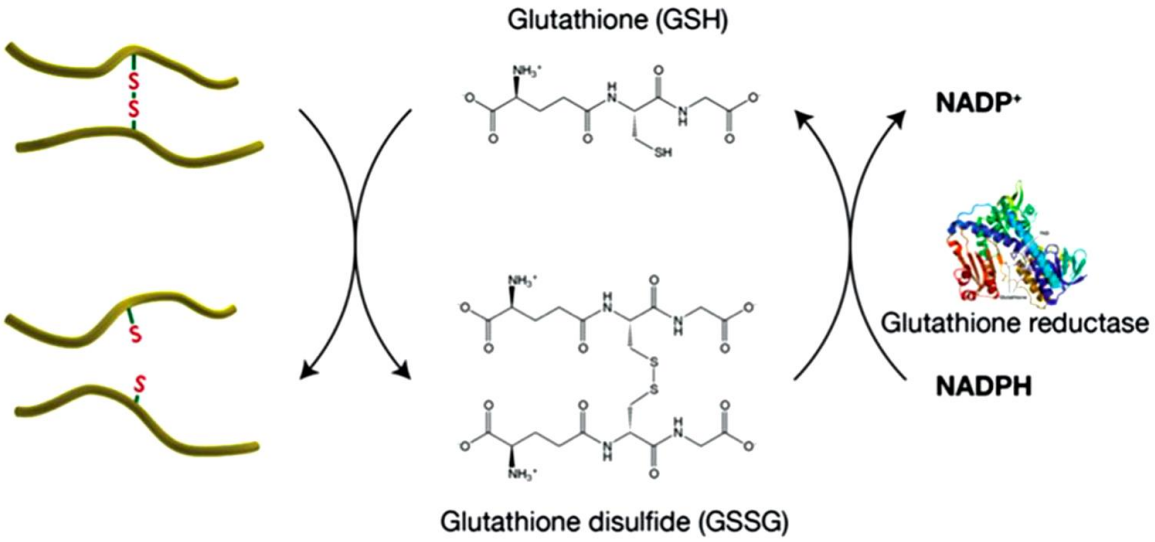

Figure 3.2.2 Schematic representation of the regeneration of glutathione (GSH) by glutathione reductase [16]

Specifically, the concentration of GSH is typically considered an indicator of the cellular reducing environment because at molecular level, it is responsible for the formation and fragmentation of disulfide bonds and the reaction with excess of reactive oxygen species (ROS) (Figure 3.2.3).

The reducing environment of tumors acts as a unique internal signal that allows redox-responsive nanocarriers and/or prodrugs to degrade in tumor cells and release loaded cargoes. There are mainly three advantages of redox-responsive nanocarriers:

- They are often stable in normal tissues, which can obviously reduce the systemic toxicity and side effects of both carriers and cargoes.
- They show a prompt response to high GSH concentration in tumor cells releasing their cargoes (usually a few minutes to hours).
- Compared to other potential sites of cargo release, the release in cytoplasm is often expected to have better therapeutic effects.

Disulfide bonds can be easily broken down by reducing glutathione into sulfhydryl groups, which causes the degradation of carriers and facilitates the release of cargoes [17].

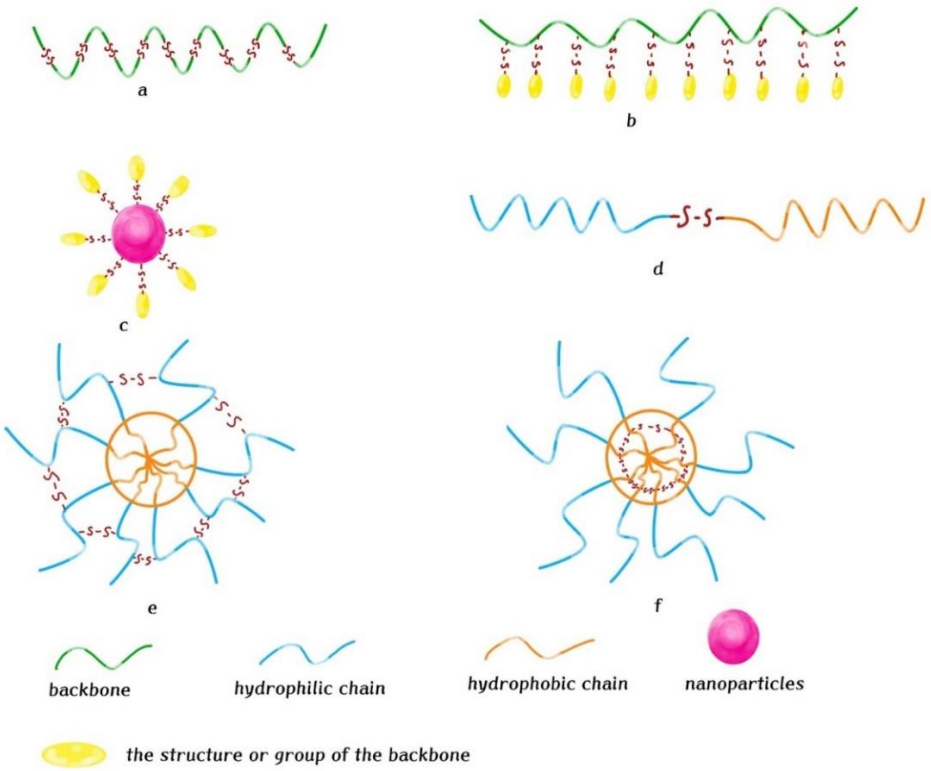

Figure 3.2.3 Scheme of the representative disulfide bonds in redox responsive delivery system

In terms of applications, mainly disulfide bonds in drug delivery systems are exploited as linkers and cross-linkers as reported in Figure 3.2.3 and detailed below:

i. Carriers with disulfide bonds in the backbone (Figure 3.2.3 a): polymeric vectors composed of many repetitive units which are degraded by the reducing environment by releasing their loads.

ii. Side chain disulfide bonds (Figure 3.2.3 b): The disulfide bond connects the hydrophobic backbone with a hydrophilic structure or vice versa. The formation of micelles can be promoted by attaching targeted groups to the spine. Redox-responsive delivery systems with disulfide bonds present in the side chain are easier to chemically modify than those with disulfide bonds in the backbone.

iii. Disulfide bonds attached to the surface of nanoparticles: (Figure 3.2.3 c): nanoparticles' surface can be properly modified with disulfide bridges to enhance their redox-responsive and targeting capabilities.

iv. Disulfide bonds can be used as ligands of the amphiphilic copolymer: by using disulfide bonds it is possible to link fractions with different pharmacological properties. The disulfide bonds, that connect hydrophilic and hydrophobic polymers to build an amphiphilic copolymer, allow to promote the formation of micelles and improve solubility (Figure 3.2.3 d).

v. Disulfide bonds can be used as cross-linkers moieties: cross-linked micelles enhance the stability during the delivery process and avoid losses of loads before reaching the tumor cell or the site of interest (Figure 3.2.3 f).

3.3 - High weight molecule-conjugate prodrug: human serum albumin (HSA)

The TME is characterized by an abnormal formation of blood vasculature with limited lymphatic drainage, thus leading to an accumulation of plasmatic protein such as human serum albumin (HSA). HSA is the most abundant protein in human blood with a concentration of about 40 mg/mL and a molecular weight of ~67 kDa; it is synthesized in the liver and approximately 13-14 g of HSA enter the body circulation each day. HSA has a remarkable ability to transport a wide variety of both endogenous and exogenous compounds, such as long-chain fatty acids, endogenous and exogeneous ligands, metal ions and drugs, thus representing a very interesting and effective natural carrier. Moreover, HSA has a biological half-life of 19 days, mostly due to its recognition by FcRn (Neonatal Fc receptor).

Since the observation that HSA can act as a selective and natural carrier, several molecules have been bound both covalently (by conjugation) and non-covalently (by specific binding) to HSA to improve anticancer treatments.

Different molecules were studied to allow the linkage of a drug with HSA. In this work, I will exclusively discuss about two of these linking moieties: the maleimide functional group and the truncated Evans Blue (EB).

Evans Blue is a tetrasodium diazo organic salt with a molecular weight of 960,8, which has a great and proved affinity for HSA (**figure 3.3.1**) [18]. When it is injected intravenously, EB becomes fully albumin-bound and only a small portion of the molecule can be found in the body (0.11%-0.31%). Thanks to this property it is possible to exploit this molecule in clinical applications [18].

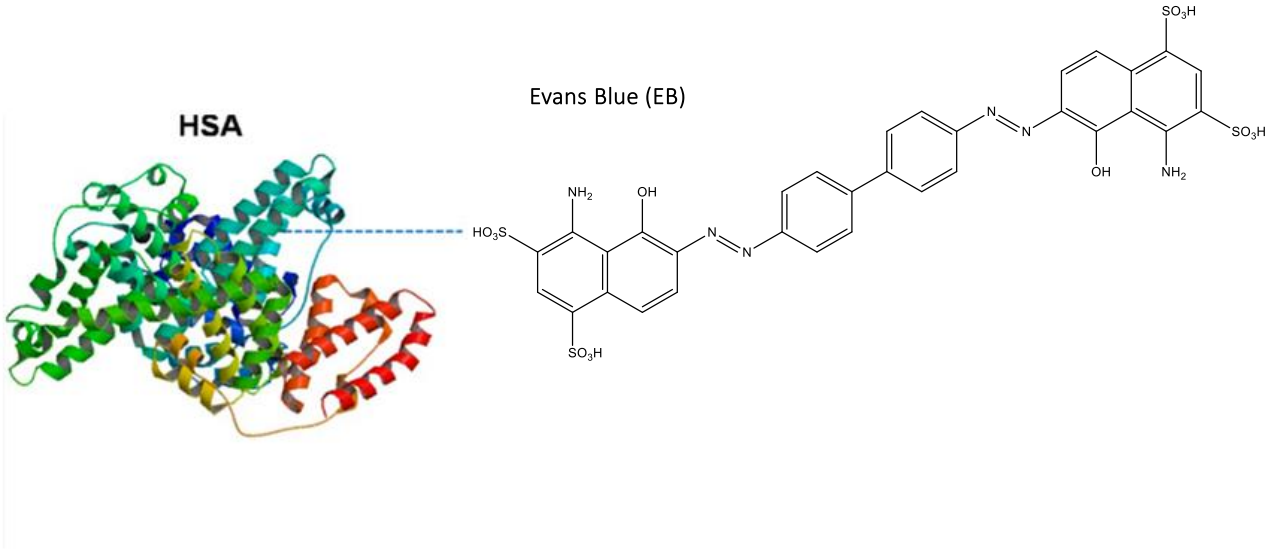

Figure 3.3.1 Chemical structure of Evans Blue

The second moiety that we have selected is the maleimide group. Kratz and colleagues pioneered this method for binding endogenous albumin. Their approach used a maleimide carboxylic hydrazone derivative of doxorubicin to form a covalent thioether bond in situ with the cysteine-34 (Cys-34) position of albumin (**figure 3.3.2**). Importantly, albumin Cys-34 represents the most abundant free thiol in the blood, and competitive side reactions with other free thiols are not a significant concern, because cysteines are typically found in nonreactive disulfide bridges. This approach is made possible by the unique properties of this amino acid residue, with approximately 70% of circulating albumin possessing the Cys-34 amino acid in its accessible form [19].

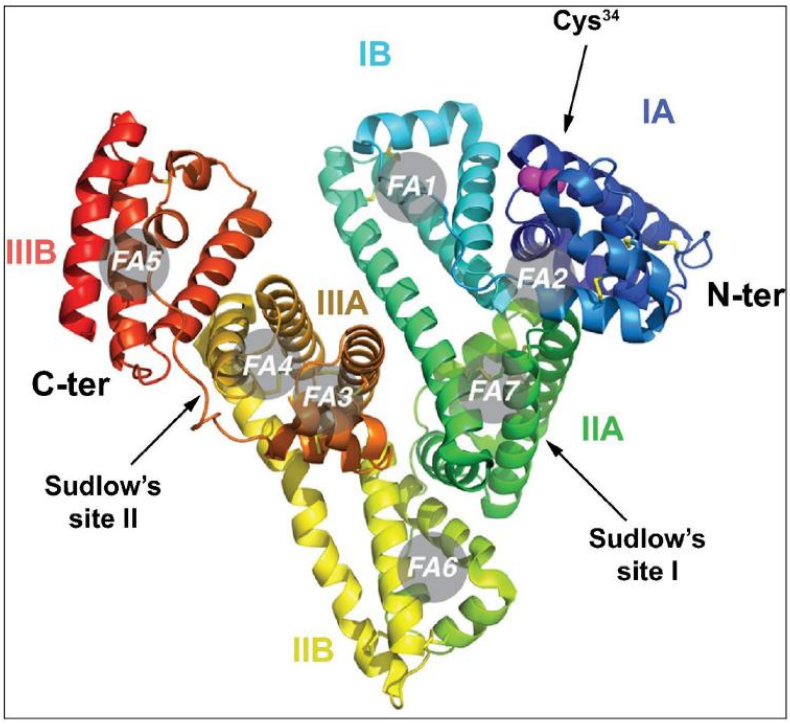

Figure 3.3.2 Crystal structure of human serum albumin [19].

4. Aim of the thesis

The aim of this thesis project was to synthetize modular prodrugs of paclitaxel (PTX) or epi-paclitaxel (EpiPTX) able to self-assemble in water and to bind endogenous serum albumin in order to exploit its intrinsic capability of tumour selective accumulation.

To this purpose, three types of molecular conjugates capable of forming HSA-binding nanoparticles were designed and synthesized:

- An EpiPTX derivative suitably modified at position C2' with an endogenous HSA PEGylated ligand (NHS-PEG-MAL). The latter was advantageously connected to the active drug, i.e., EpiPTX, via a bioresponsive disulfide bridge able of releasing EpiPTX under reductive conditions.

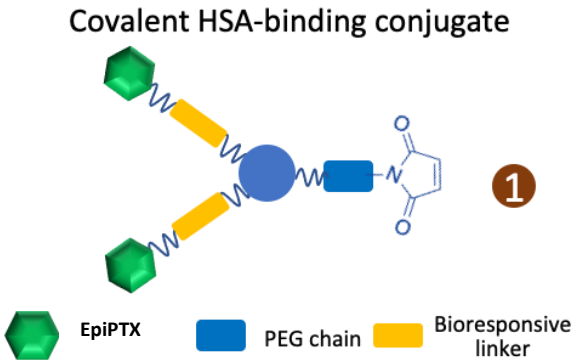

- PTX and EpiPTX bioresponsive monomers and dimers were designed and synthesized carrying tEB as non-covalent HSA-binding moiety. In addition, different kind of connections between tEB and PTX were explored, i.e., ester and carbonate bonds, to determine the best-performing releasing and selective conjugate.

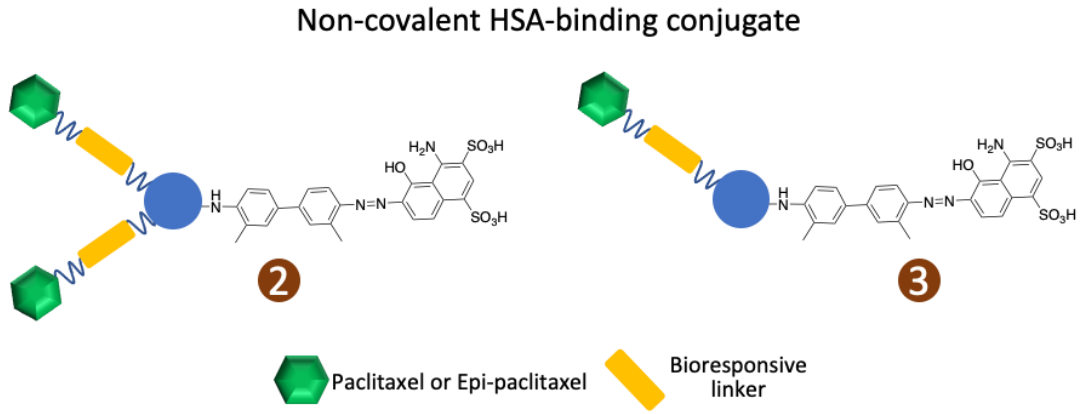

5. Results and discussion

5.1 - Synthesis of covalently HSA-binding prodrugs

The first part of my thesis was dedicated to the synthesis of different PTX and EpiPTX monomeric and dimeric bioresponsive prodrugs, with the aim of defining the best candidates for nanoparticles formation.

5.2 - Synthesis of EpiPTX-SS-PEGMAL

During the first part of my work, I focused my activity on the preparation of the EpiPTX-SS-PEGMAL derivative (**6**) following the synthetic strategy depicted in **Scheme 1**.

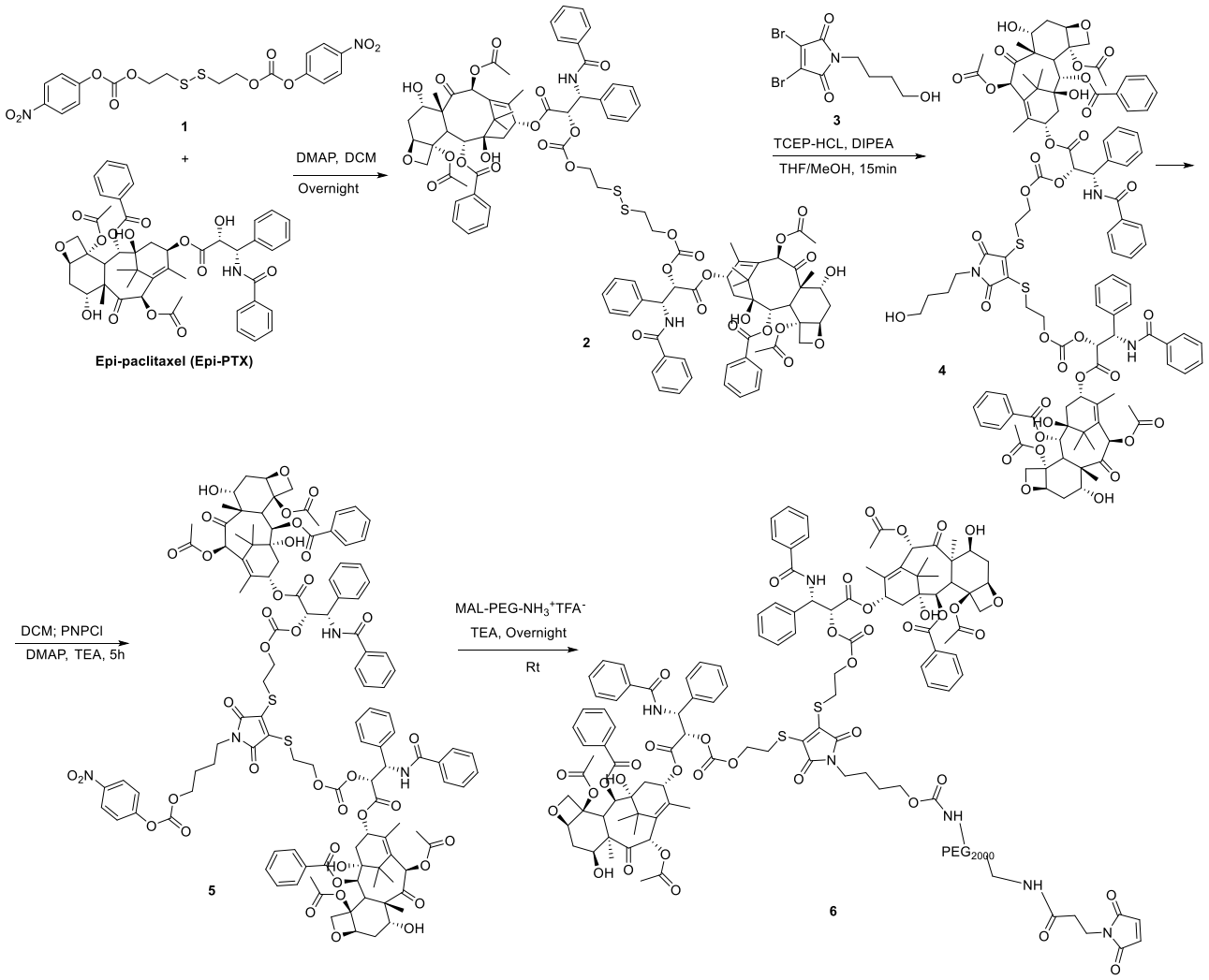

Scheme 1 – General synthetic strategy for the preparation of compound 6.

Indeed, EpiPTX chemically differs from PTX only by the stereochemistry of C7 position, thus allowing to setup all procedures on this less expansive molecule. Indeed, the C7 stereogenic centre in the taxane ring of PTX is notably labile and can readily undergo epimerization in aqueous environment, resulting in 7-epi-paclitaxel (EpiPTX), a biologically active and thermodynamically more stable PTX stereoisomer. EpiPTX exhibits properties comparable to those of Taxol both on cells and on in vitro microtubule polymerization [10].

As stated before, the EpiPTX-SS-PEGMAL conjugate was designed to covalently bound circulating HSA through the reaction of the maleimide group with the SH of the Cys 34 amino acid present on the HSA backbone (Figure 3.3.2).

As shown in Scheme 1, the first step of the synthesis involved the formation of the EpiPTX-SS-EpiPTX dimer (2) which was achieved through a substitution reaction following a literature procedure [20]. By reacting compound 1 (see experimental section) with EpiPTX in the presence of a catalytic amount of 4-dimethyl amino pyridine (DMAP), the EpiPTX 2'-OH functional group attacks the CO group through an esterification process. After a night at room temperature, compound 2 was isolated by flash column chromatography in 78% yield as a white solid (Scheme 2)

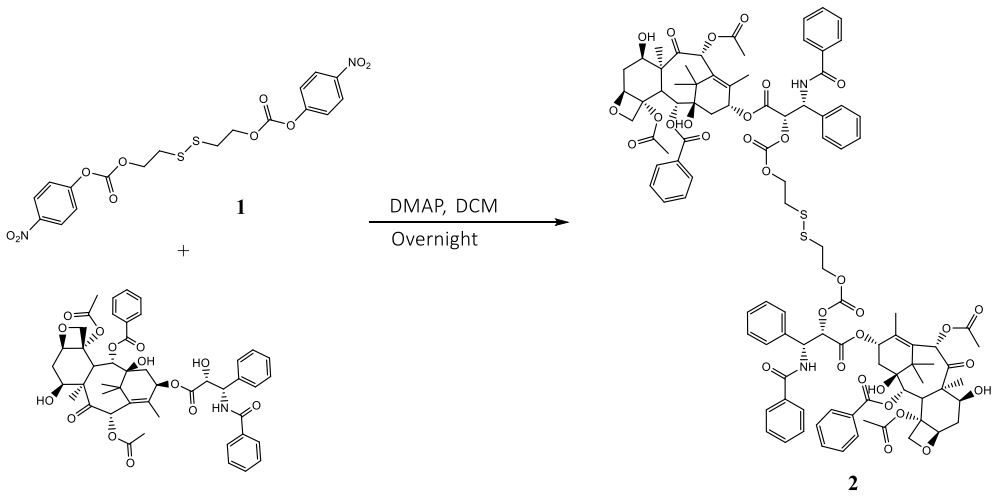

Scheme 2 – Synthesis of Epi-PTX dimer 2.

The structure of compound 2 was confirmed by ^{1}H-NMR analysis showing the appearance of the -CH_2 signals at 2.88 (triplet) and 4.34 (multiplet) corresponding to the protons of the linker chain (Figure 5.1).

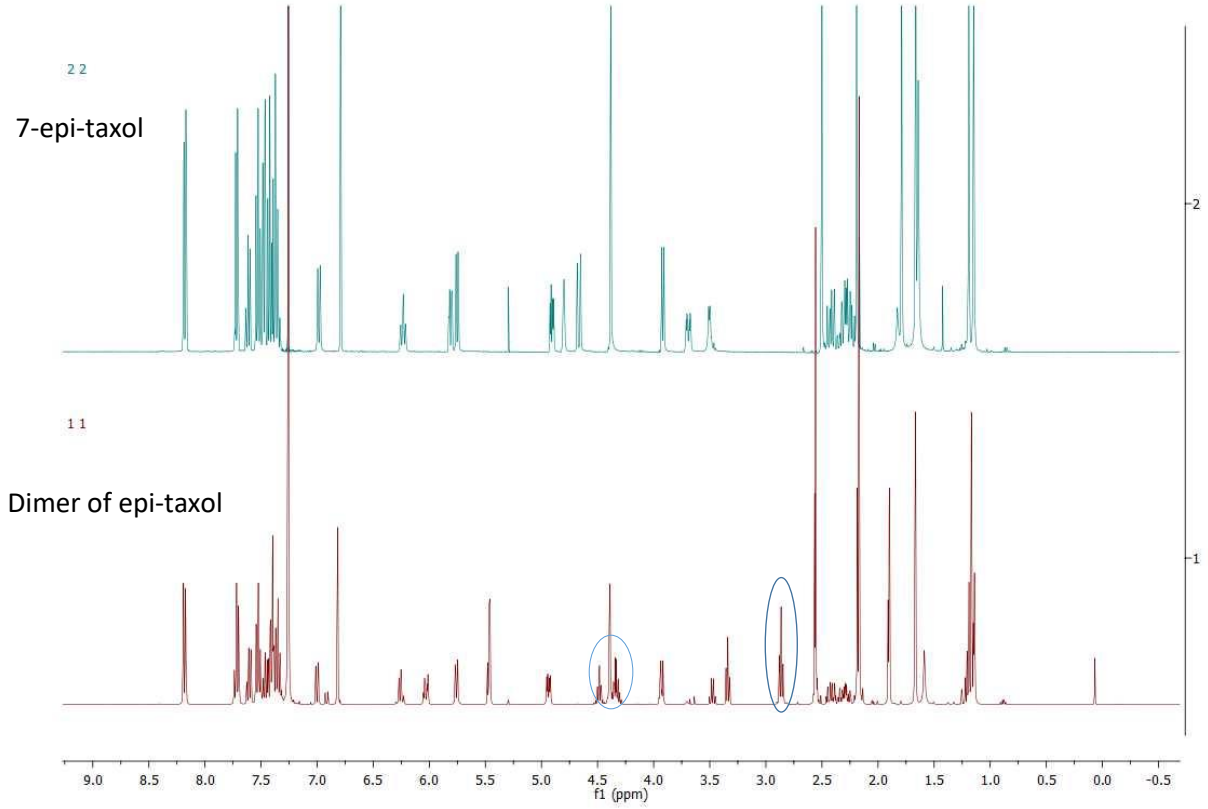

Figure 5.1 *[1]HNMR spectra comparison between 7-epi-Taxol and the dimer of epiPTX carbonate dimer.*

The following step included the synthesis of the derivative **4** (Scheme 3) which was achieved following a literature procedure suitably modified in order to optimize the reaction yield [21].Therefore, compound **2** was conjugated to compound **3** (see experimental section) in the presence of tris(2-carboxyethyl)phosphine hydrochloride (TCEP-HCl), N,N-Diisopropylethylamine (DIPEA) to neutralize the HCl present in the reaction mixture, methanol (MeOH) and tetrahydrofuran (THF) (1:3) as solvents. The phosphorus atom of TCEP attacks one sulphur atom along the S-S bond. A thioalkoxyphosphonium cation and a sulfhydryl anion are formed, then a rapid hydrolysis releases the second sulfhydryl molecule and the phosphine oxide. It follows a substitution of the two bromines by the sulfhydryl molecule to afford the desired compound. After 15 minutes at room temperature, solvents were removed and compound **4** was isolated by flash column chromatography in 40% yield.

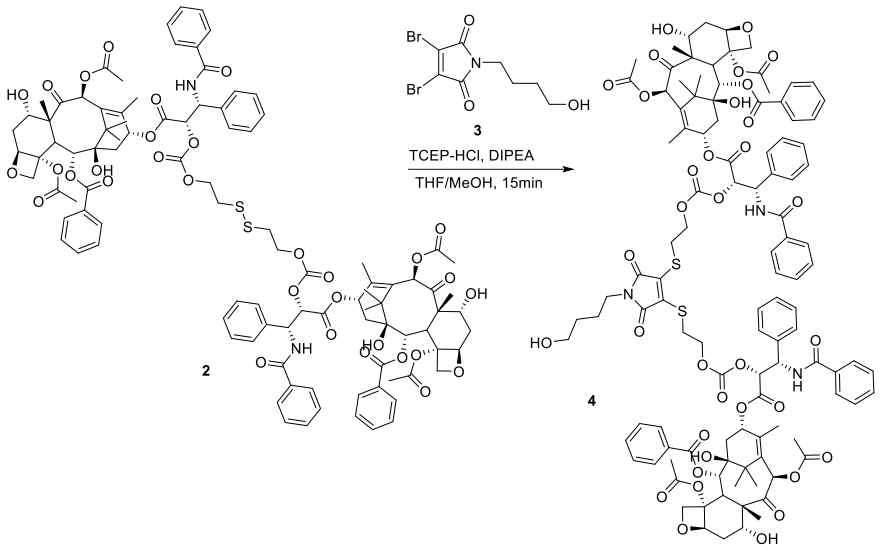

*Scheme 3 – Synthesis of derivative **4**.*

Interestingly, compound **4** emits fluorescence in the green region of the UV-Vis spectra (**Figure 5.2**). This feature could be of particular interest for biomedical application, allowing the in vitro tracking of the compound's internalization and fate.

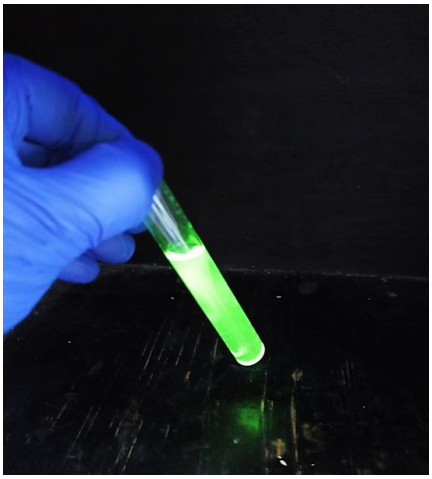

***Figure 5.2** Fluorescence emission of compound **4** under UV irradiation*

The synthesis of the $(EpiPTX)_2$-SS-$(CH_2)_4$-MAL conjugate (**5**) was obtained by reacting compound **4** with 4-nitrophenyl-chloroformate (PNP-Cl) in presence of triethylamine (TEA) as auxiliary base, in order to neutralize the HCl produced during the reaction, as catalyst for the esterification it was used DMAP, and DCM as the reaction solvent. After 5 hours at room temperature, compound **5** was isolated by flash column chromatography in 40% yield.

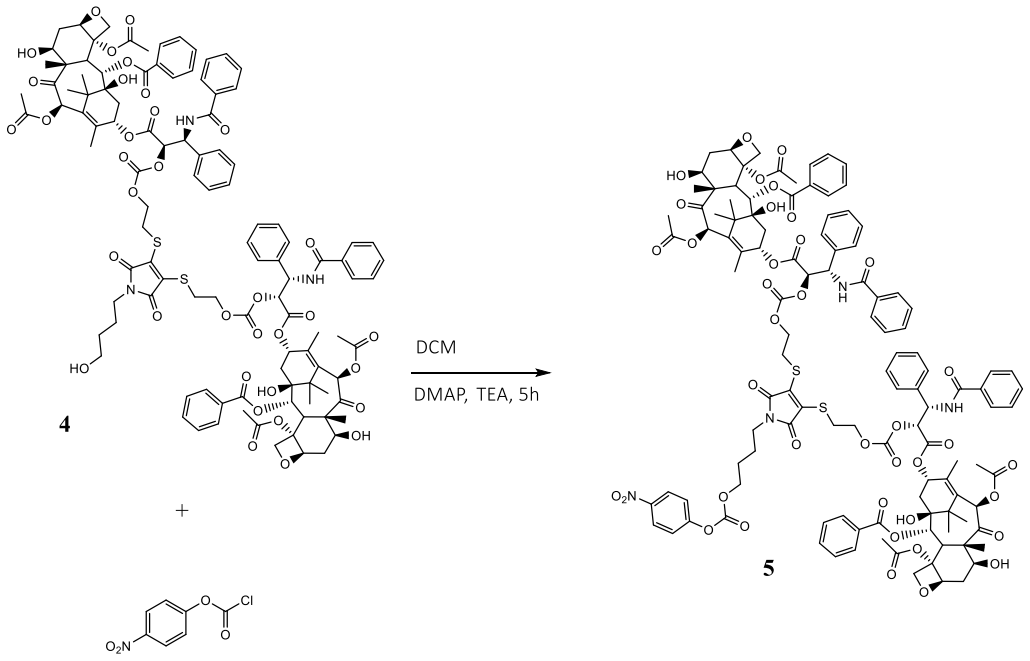

Scheme 4 – Synthesis of derivative 5.

To obtain our desired product (6) a coupling reaction was performed between compound 5, having the phenolate as a good leaving group, and the PEGylated albumin binder, MAL-PEG$_{2000}$-NH$_3^+$TFA$^-$, in the presence of TEA. The crude material was purified via dialysis (3500 MWCO) against water/DMSO (0.1%) to separate compound 6 from unreacted MAL-PEG$_{2000}$-NH$_3^+$TFA$^-$ and other reagents.

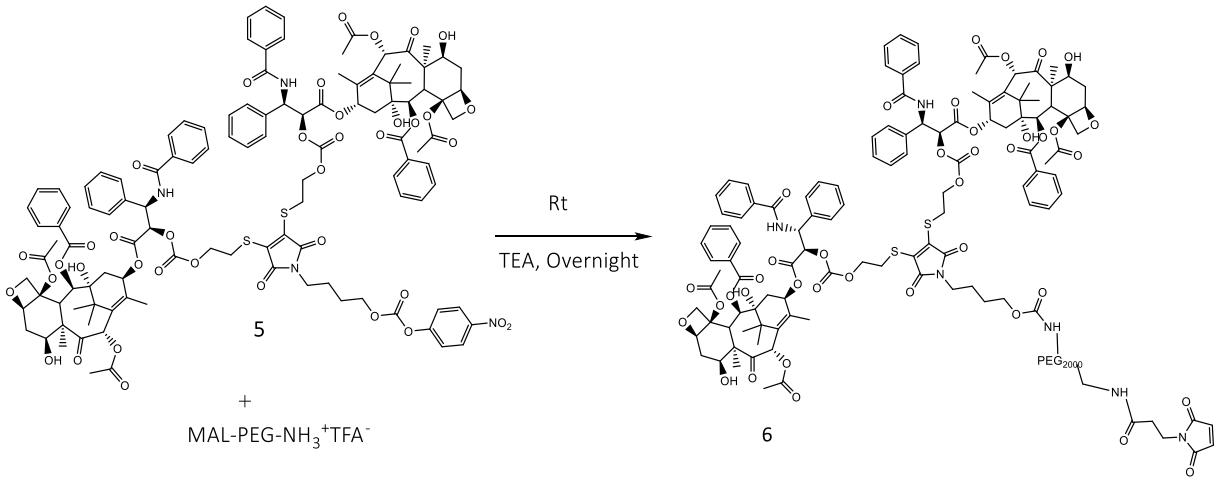

Scheme 5 – Synthesis of final compound 6.

Similarly, derivative (PTX)$_2$-SS-(CH$_2$)$_4$OH (compound 8) was obtained by following the same procedures previously reported for EpiPTX, with the aim of assessing the feasibility of the synthetic strategy on the actual drug, e.g., PTX (Scheme 6).

In particular, the dimer **7** was obtained in 83 % isolated yield (see exp section) while the following compound **8** was isolated from the crude mixture in 47% yield. Lastly, we obtained compound **9** by reaction of compound **8** with 4-nitrophenyl-chloroformate which afforded the corresponding derivative **9** in 47% isolated yield.

Unfortunately, due to time constrains, it was not possible to perform the final coupling reaction between compound **9** and MAL-PEG_{2000}-$NH_3^+TFA^-$. These experiments are now ongoing at the research group where I performed this thesis project.

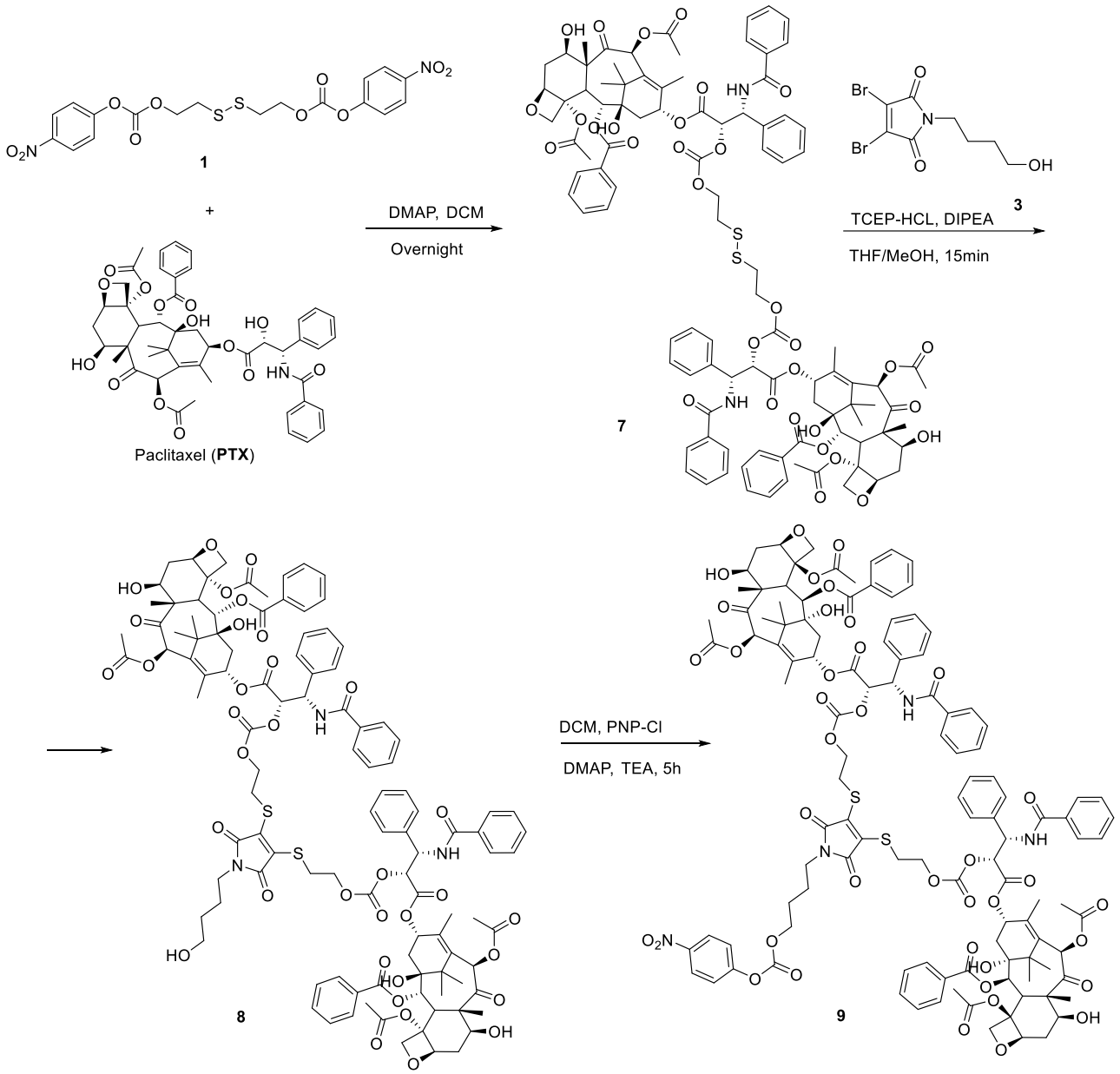

Scheme 6 – Reaction scheme for the synthesis of derivative 9.

5.3 - Synthesis of non-covalent HSA binding prodrugs with ESTER bond

In the second part of my thesis work, I focused my activity on the preparation of mono- and dimeric bioresponsive prodrugs bearing the truncated Evans Blue (tEB) pedant for the non-covalent in situ binding of circulating HSA. In particular, the first derivative being prepared was the EpiPTXsstEB derivative **17** characterized by an ester bond between the drug and the bioresponsive linker (**Scheme 7**).

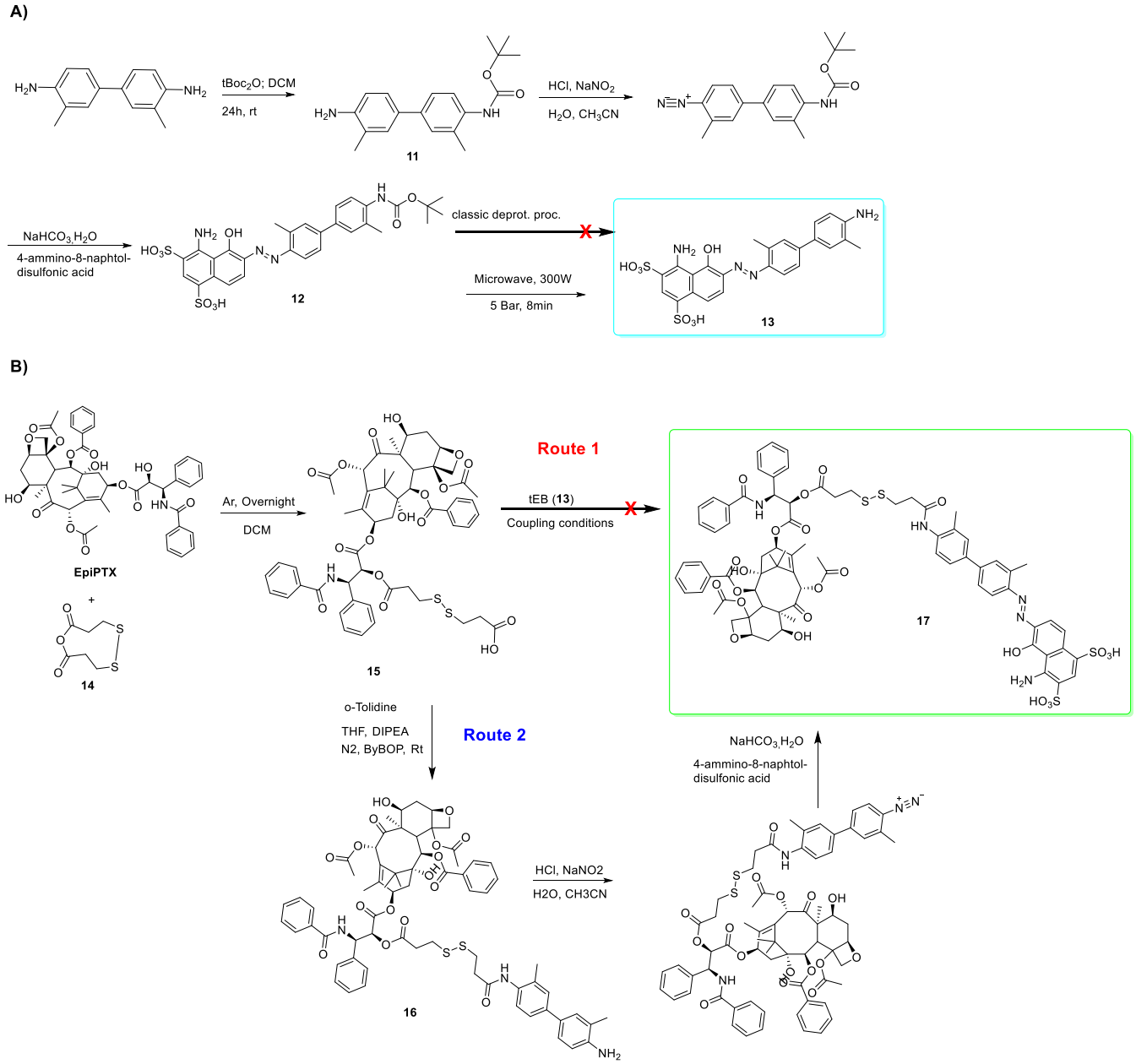

Scheme 7. General scheme for the synthesis of conjugate 17

In the first step of this synthetic procedure, we prepared the tEB pendant (**Scheme 7A and Scheme 8**). At first, 3,3-dimethylbenzidine (o-tolidine) was mono-protected with di-tert-butyl dicarbonate

(BOC_2O). The reaction was performed under anhydrous condition for 24 h at room temperature affording compound **11** in 46% yield Fare clic o toccare qui per immettere il testo.Notably, we also obtained a 12% of di-protected compound, that could be selectively mono-deprotected and used for further experiments.

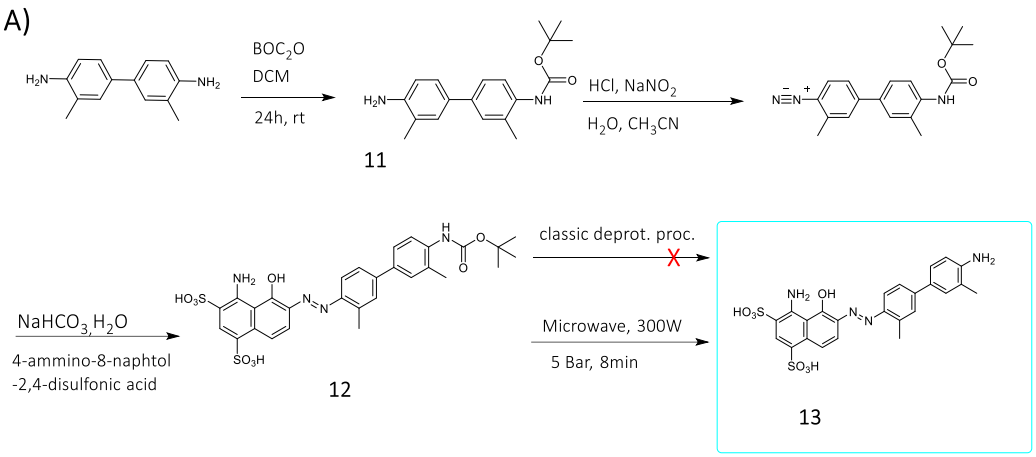

Scheme 8 – Synthesis of compound 13

Derivative **11** was then treated under diaziotation conditions by first reacting with $NaNO_2$ and HCl in acetonitrile following the experimental procedure reported in the experimental section. The salt formation was evident when the colour of the solution become bright orange. Then, the azo-coupling reaction was performed at 0 °C between the intermediate and 1-amino-8-naphthol-2,4-disulfonic acid dissolved in a solution of H_2O and $NaHCO_3$ to obtain the diazo-compound **12** in quantitative yield. The crude material was freeze dried to remove water and acetonitrile and characterized by ^{1}H-NMR. The last step of the procedure involved the deprotection of compound **12** to the corresponding tEB derivative **13** (**Scheme 8**). To do so, we first followed literature procedures indicating the use of trifluoro acetic acid (TFA) and different cations scavengers, such as thioanisole and 1,2-ethandithiol, to achieve the product formation [23]. Despite quite effective in affording the desired deprotected compound, its purification from scavenging compounds is tedious and not quantitative. Therefore, we decided to setup an alternative and more eco-friendly MW-based procedure, applied in the literature to other kind of molecules [24] which allowed the straightforward deprotection of compound **12** (**Scheme 8**). Amazingly, by treating compound **12** with water only under a pression of 5 Bar and a power of 300 W for 8 min, tEB (**13**) was obtained in quantitative yield as pure dark red powder upon freeze drying.

The second phase of the procedure focused on the preparation of the final derivative **17**. To this end, I first prepared the EpiPTX monomeric acid, e.g., EpiPTX-ss-COOH (**15**) that was obtained through a condensation reaction via the esterification of the 2'-OH functional group with the 1,5,6-oxadithionane-2,9-dione (DTPDA) anhydride (compound **14**) in the presence of TEA, a catalytic amount of DMAP and DCM as the reaction solvent under argon atmosphere. After reacting overnight, the product (compound **15**) was recovered and purified using flash chromatography with a conversion yield of 77% (**Scheme 9**).

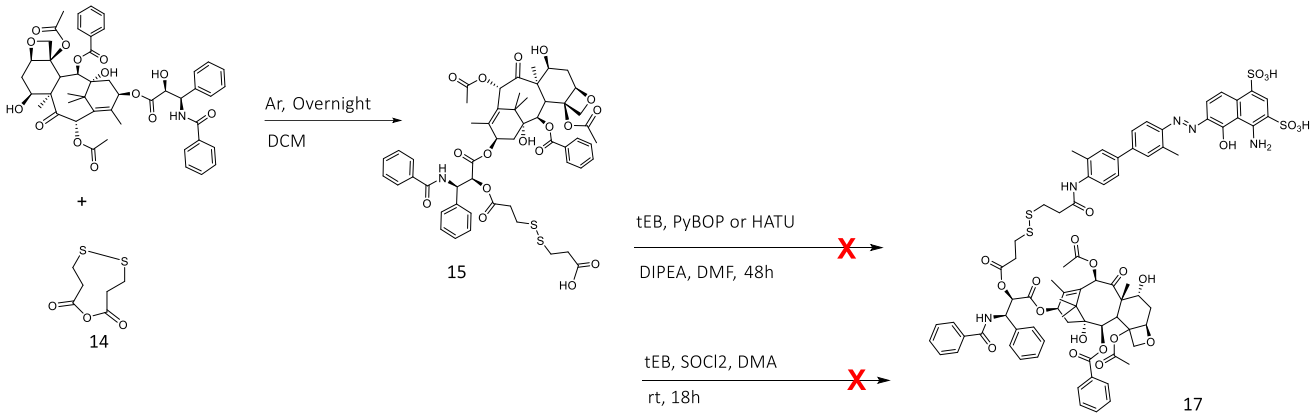

Scheme 9 – Attempted synthesis of compound 17.

The following step involved the coupling reaction between the carboxylic acid moiety of compound **15** and the amino group present on the tEB by using different coupling agents (**Scheme 9**).

Details on the reaction conditions applied for accomplishing this reaction are reported in **Table 1**. Unfortunately, none of the attempted conditions allowed to isolate the desired product, most probably due to the scarce reactivity of the NH_2 group on the tEB molecule.

Reagents and equivalents	Time	Solvent (mL)	References
EpiPTX-COOH (**14**) (2eq); tEB (1eq) DIPEA (10 eq); Hexafluorophosphate Aza-benzotriazole Tetramethyl Uronium (HATU) (2eq)	48 h	DMF (2mL)	(S.M.Mallikarjuna et al. 2017), [20]
PTX-COOH (**14**) (1eq); tEB (0.7 eq) DIPEA (10eq); benzotriazol-1-yloxytripyrrolidinophosphonium hexafluorophosphate (PyBOP) (1eq)	48 h	DMF (1.5mL)	(F.Zhang et al., 2017), [26]
PTX-COOH (**14**) (1eq) tEB (0.8 eq); $SOCl_2$ (2.12 eq)	18h	DMA (1mL)	(A. Guerrini et al.,2017), [27]

Table 1 Tentative procedures for the synthesis of the prodrug

Based on these results, we decided to apply a different approach to achieve the synthesis of the desired compound, **17**. In particular, we first reacted the EpiPTXssCOOH derivative **15** with o-tolidine. The reaction was performed under anhydrous conditions at room temperature in the presence of DIPEA, PyBOP as coupling agent and THF as solvent. After 1.30 h the product was recovered and purified by flash chromatography with a yield of 32% (**Scheme 10**).

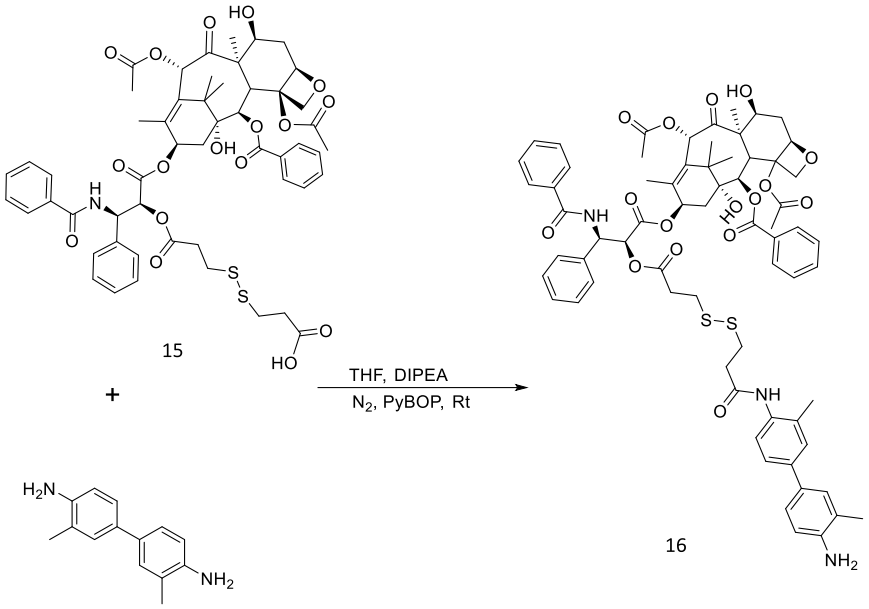

Scheme 10 - Reaction scheme of the synthesis of EpiPTX-SS-TOL

Afterwards, by following the same diazotation conditions reported previously for the preparation of tEB, we obtained compound **17** in 40% yield (**Scheme 11**).

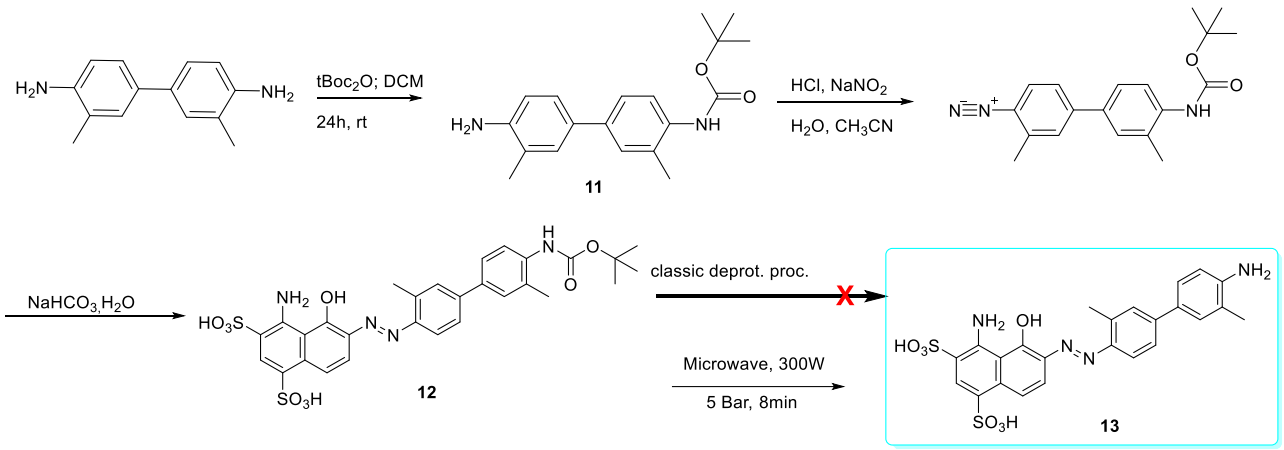

Scheme 11 - Reaction scheme of the synthesis of EpiPTX-SS-tEB (17)

Due to the presence of water and acetonitrile, the crude product was lyophilized to obtain a violet powder. To remove all salts present in the reaction mixture, the powder was dissolved in water and

MeOH and purified by dialysis (1KDa MWCO) first against water/DMSO (3%) followed by water only, and further freeze dried to afford the pure compound which was characterized by ^{1}H-NMR.

The same reaction procedure was followed for the synthesis of the compound PTX-SS-Tol (Scheme 12). In particular, the monomer **18** was obtained with a conversion yield of 90% (see exp section) while the following (compound **19**) was isolated from the crude mixture in 45% yield. Unfortunately, due to time constrains it was not possible to perform the last diazotation step on compound **19**. These experiments are currently ongoing at the CNR group where I performed my thesis work.

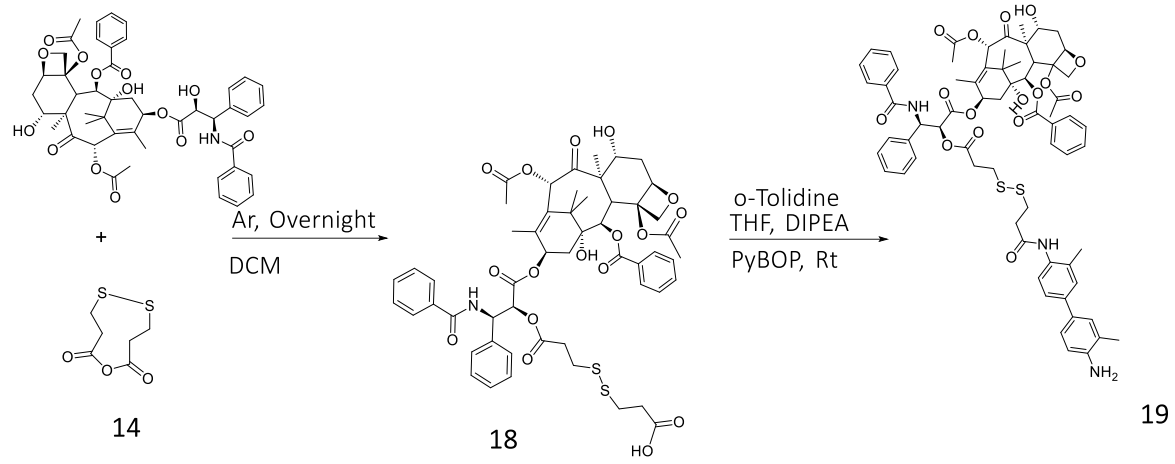

Scheme 12 – Synthesis of derivative 19

5.4 - Synthesis of the non-covalent HSA binding PTX prodrugs bearing a CARBONATE bond

We next synthesized a second non-covalent HSA binding PTX prodrug, that differs from the ones previously described by the presence of a carbonate group instead of an ester moiety, between the drug, e.g., PTX, and the bioresponsive linker (Scheme 13).

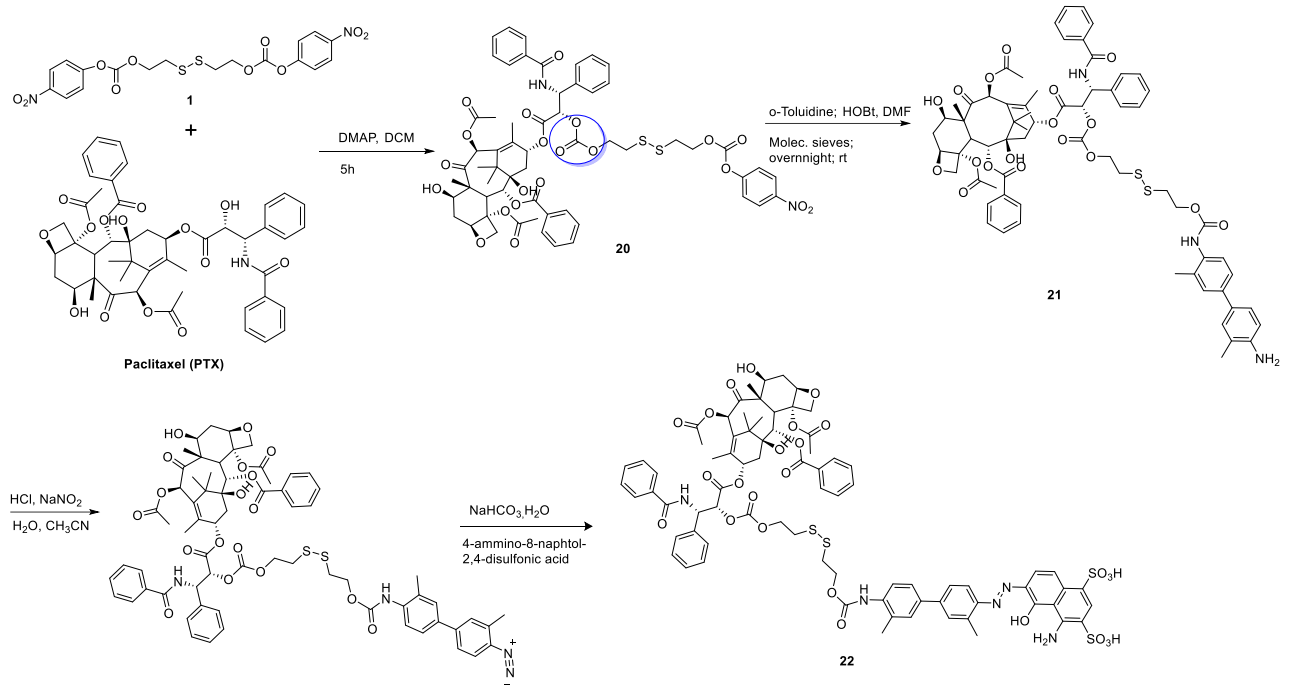

Scheme 13 – General synthetic strategy for the synthesis of derivative 22

As shown in Scheme 13, the first step of the synthesis involved the formation of the PTX-SS-PNP derivative (20). This was achieved through a slightly modified literature procedure in order to avoid or limit the formation of the dimer [20]. Indeed, by reacting compound 1 (see experimental section) with PTX in the presence of a catalytic amount of 4-dimethyl amino pyridine (DMAP), the PTX 2'-OH functional group attacks the CO group of the internal chain and through a transesterification process compound 20 is formed. After a night at room temperature, compound 20 was isolated by flash column chromatography in 54% yield as a white solid.

In the following step, compound 21 was attained through a coupling reaction between o-tolidine and the activated PTX monomer (20) following a literature procedure [28]. The reaction was performed under anhydrous conditions at room temperature in the presence of 1-hydroxybenzotriazole (HOBt), molecular sieves (4 Å) and DMF as solvents. After a night at room temperature the product was recovered and purified by flash chromatography with a yield of 47% (Scheme 13).

The last step (Scheme 14) was the diazotation process that was performed following the same procedure already described for the preparation of compound 17. Compound 22 was purified by dialysis followed by freeze drying. To improve compound purity, the freeze-dried powder was also purified by flash column chromatography and then analysed through ^{1}H-NMR spectroscopy.

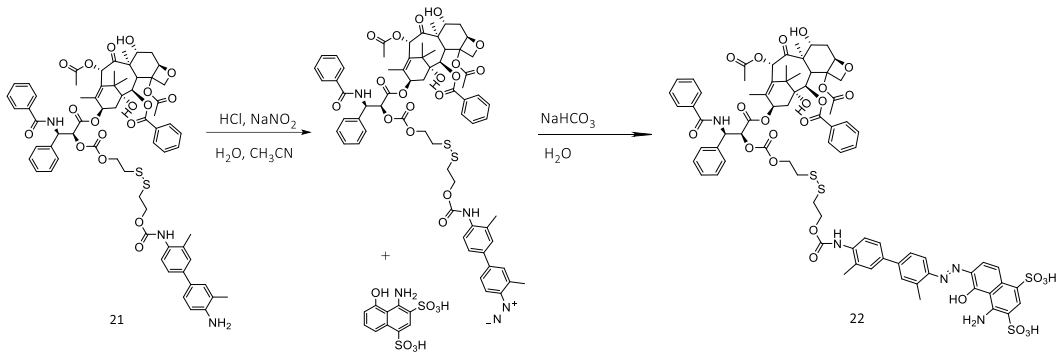

Scheme 14 - Synthesis of derivative 22

Lastly, we attempted the synthesis of the PTX dimeric prodrug **10** (Scheme 16) starting from the previously described compound **9**.

The synthesis of the compound **10** was attained through a coupling reaction between o-tolidine and compound **9** following a literature procedure [28] as previously described. The reaction was performed under anhydrous conditions at room temperature in molecular sieves, HOBt as coupling agent and THF as solvent. After a night at room temperature the product was recovered and purified by flash chromatography in 30% yield.

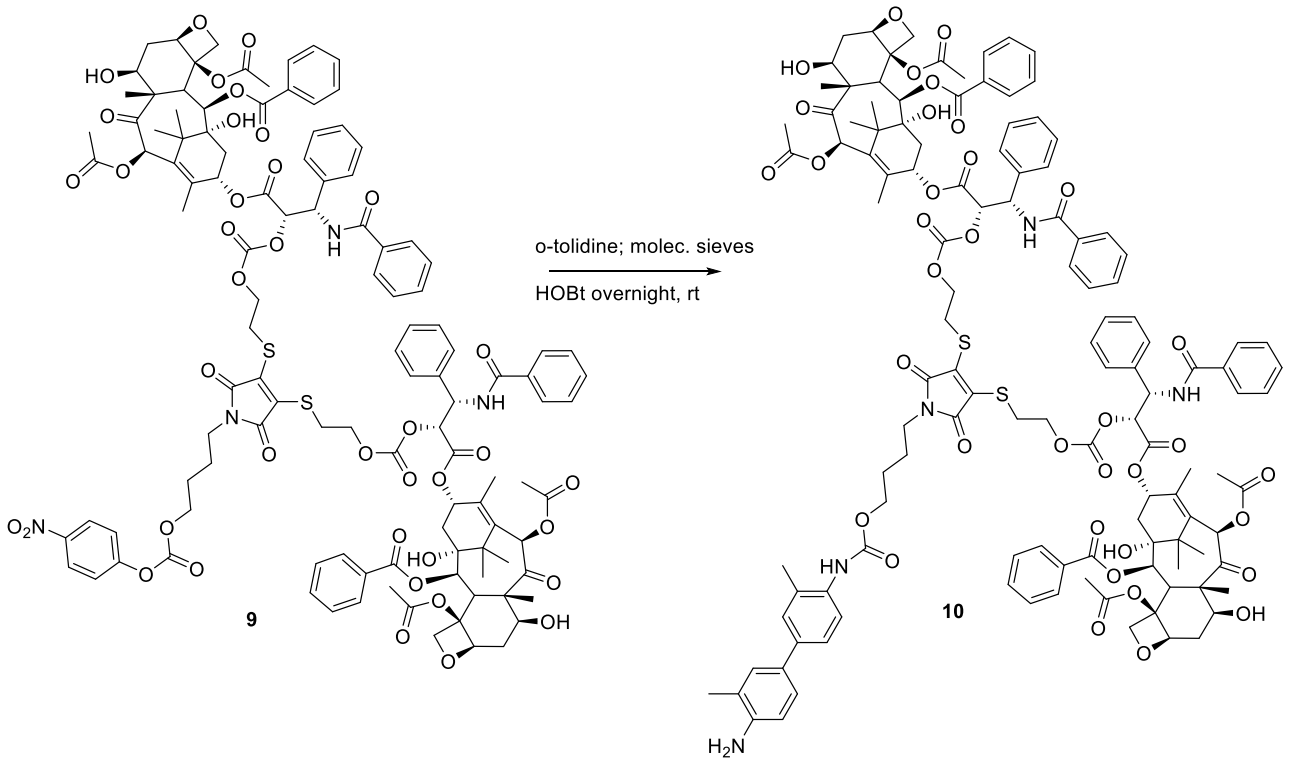

*Scheme 16 – Synthesis of compound **10**.*

In the future compound **10** will be treated under diazotation conditions to afford another potential non-covalent HSA binding prodrug for nanoparticles formation.

5.5 – Bioresponsive nanoparticles preparation

Different kinds of nanoparticles were subsequently prepared based on previously synthesized prodrugs. In particular, derivatives **6**, **17** and **22** (**Figure 5.5**) were selected to perform these preliminary experiments.

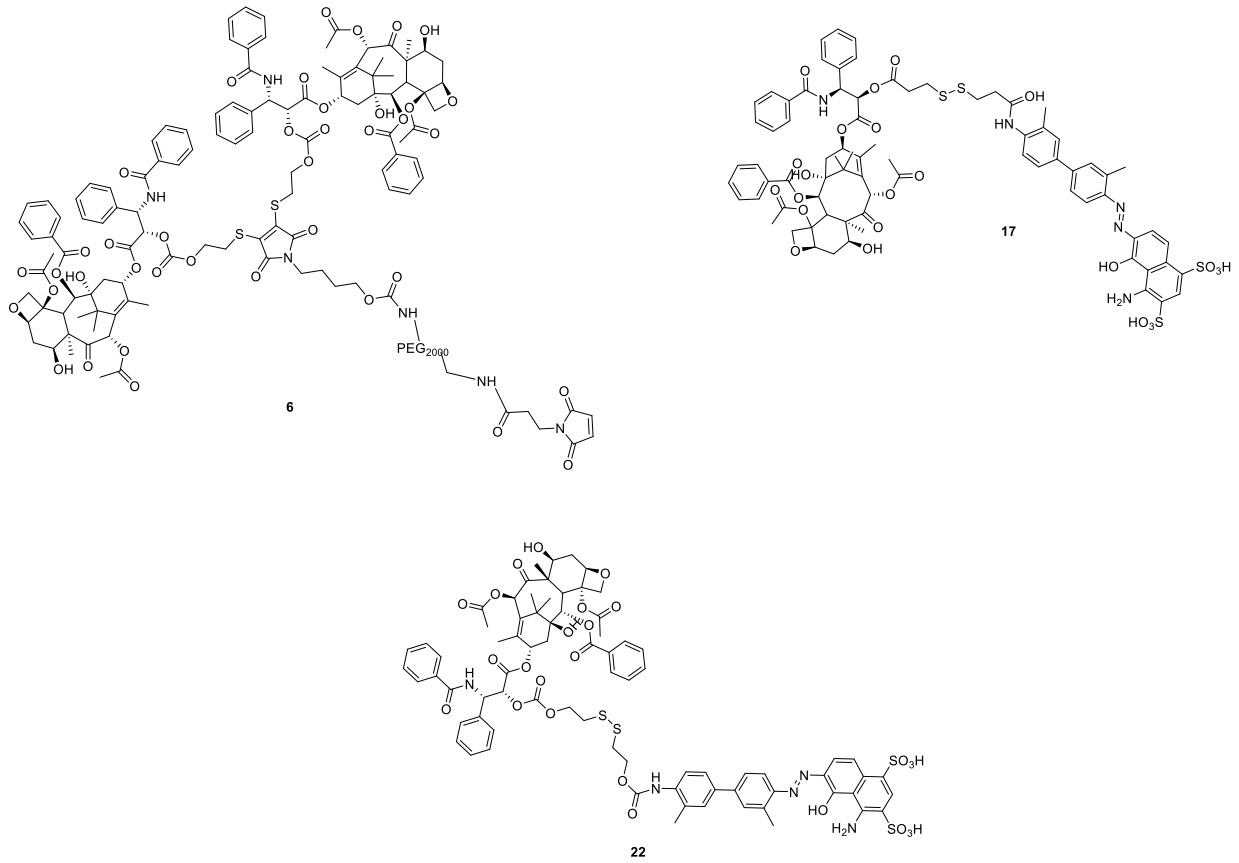

Figure 5.5. Chemical structures of compounds **6**, **17** and **22** used for nanoparticles preparation

Nanoparticles were prepared trough the nanoprecipitation method which includes dissolving the prodrug in a tiny amount of organic solvent (miscible in water) and then inject this solution into ultrapure water under vigorous stirring. At this point, if the molecule possesses the appropriate self-assembling and amphiphilic properties, it will spontaneously generate nanoparticles of different dimensions and stability.

5.5.1. Nanoparticles preparation from covalently HSA binding PTX prodrug ***6.***

As previously mentioned, nanoprecipitation was employed for the preparation of *(EpiPTX)$_2$SS-(CH$_2$)$_4$-PEG-MAL* nanoparticles, @NPs-**6** (see experimental section) with a hydrodynamic diameter, measured by dynamic light scattering (DLS), of 103 nm and a polydispersity index (PDI) of 0.4.

A preliminary stability study was performed in phosphate buffer saline (PBS) by keeping the sample at 37°C for 24 h, demonstrating that @NP-**6** are stable under these conditions with a slight decrease of the hydrodynamic diameter (90 nm).

As shown in Figure 5.3, once irradiated with UV light, the nanoparticles solution shows a moderate turbidity and a homogeneous fluorescence distribution, thus empirically confirming a suitable particles' dispersion.

From these data we can infer that the bioresponsive prodrug **6** efficiently forms nanoparticles in water, thus possibly being a very promising candidate for the preparation of novel PTX-bioresponsive nanosystems alone or in combination with other drugs.

More studies will be performed to fully characterize these systems in terms of physical-chemical properties, ability to load other active ingredients, TME-mediated release, ability to covalently bind HSA and in vitro efficacy against breast cancer cells.

*Figure 5.3 Fluorescence emission of @NPs-**6** under UV irradiation.*

*5.5.2. Nanoparticles preparation from covalently HSA binding PTX prodrug **17**.*

We next evaluated the ability of compound **17** of forming nanoparticles in water, e.g., @NPs-**17**. To this end, the nanoprecipitation method was applied in which compound **17** was dissolved in ethanol at a concentration 1.5 mg/mL. After 5 minutes under stirring, half of the solution was taken and inserted in i) a cuvette containing 1mL of ultrapure H_2O or ii) with 1mL of a BSA solution (30 mg/mL), to have a final volume of 1.8 mL and a nanoparticles concentration of 0.4mg/mL. Our preliminary results indicate that derivative **17** has a good propensity of forming nanoparticles with an average hydrodynamic of 199 nm and an average PDI of 0.8.

To evaluate @NPs-**17** stability, the solution was kept in the oven at 37°C up to 4 h. Preliminary results are reported in **Table 3**, indicating that @NPs-**17** are stable in all tested conditions, and, as expected,

the presence of BSA seems to contribute to increasing their stability while reducing their hydrodynamic diameter. This behaviour might indicate that @NPs-**17** bind to BSA providing the formation of smaller and BSA-coated nanoparticles, thus indirectly demonstrating the ability of the tEB moiety to tightly interact with serum proteins and paving the way for these nanosystems to be efficiently transported by HSA once injected in the blood stream.

Table 3 - DLS analysis of the nanoparticles in aqueous environment and in BSA solution after 2 and 4h in the heater

Sample (concentration, time)	Diameter (nm)
11 *(0.4mg/mL in H2O 2h)*	196.6 ± 1.74
11 *(0.4mg/mL in BSA 2h)*	159.7 ± 7.07
11 *(0.4mg/mL in H2O 4h)*	194.6 ± 1.83
11 *(0.4mg/mL in BSA 4h)*	164.1 ± 7.15

5.5.3. Nanoparticles preparation from covalently HSA binding PTX prodrug ***22.***

In the last part of my thesis work, I made the first attempts to produce nanoparticles with the prodrug **22** (@NPs-**22**) differing from derivative **17** by the presence of the carbonate bond between PTX and the HSA-binding and bioresponsive linker. To this end, the nanoprecipitation method was applied in which compound **22** was dissolved in EtOH at a concentration of 1.5 mg/mL and the obtained solution was added dropwise to water under vigorous stirring. After few minutes under stirring, the solution was taken and inserted in a cuvette containing i) 1mL of ultrapure H_2O or ii) 1mL of a BSA solution (30 mg/mL). At this point the hydrodynamic diameter was measured by DLS indicating an average diameter of 110 nm (H_2O), and 102 nm (BSA solution).

Afterwards, ethanol was removed under controlled rotary evaporation, and changes in @NPs-**22** size was checked through DLS analysis. A significant increase in diameter was observe for @NPs-**22** in water going from 110 to 254 nm, probably due to nanoparticles partial aggregation. Conversely, the diameter of particles dispersed in BSA solution was stable (101 nm), further confirming the effect of serum proteins on their stability.

These preliminary results indicate that ethanol is an appropriate solvent for @NPs-**22** preparation and that the presence of serum protein. e.g., BSA, highly contribute to particles' stabilization.

To further verify @NPs-**22** stability in BSA solution, the sample was kept at 37°C for 2h and the diameter checked by DLS analysis which accounted for an average diameter of 81 nm, indicating a

good nanoparticles stability. Overall, these preliminary data allow to conclude that, once exposed to BSA, our prodrugs-based nanoparticles effectively bind to the protein, thus increasing their stability and propensity to act as drug carriers (Figure 5.4).

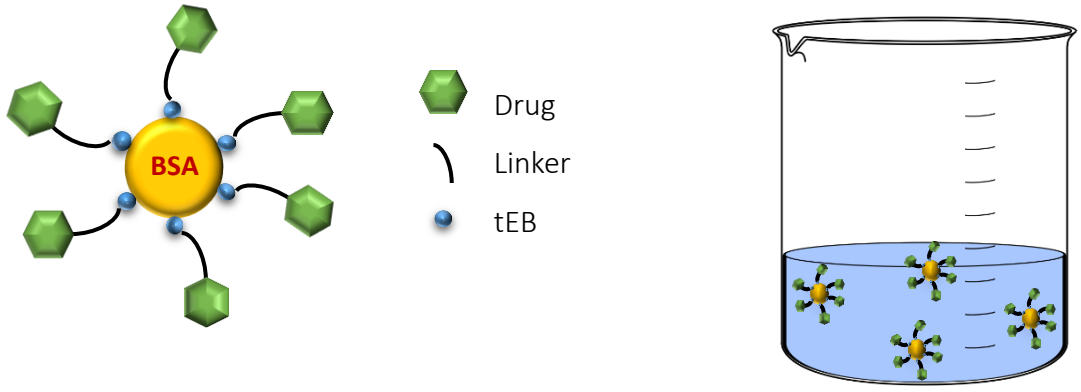

Figure 5.4 Schematic interaction between the prodrugs and BSA

6. Conclusions and future work

To conclude, in this work I synthesized for the first time different mono- and dimeric epi-paclitaxel and paclitaxel prodrugs featured with specific antennas (figure 6.1) for the covalent and non-covalent binding of HSA, as endogenous, natural and selective transporter towards the tumor tissue.

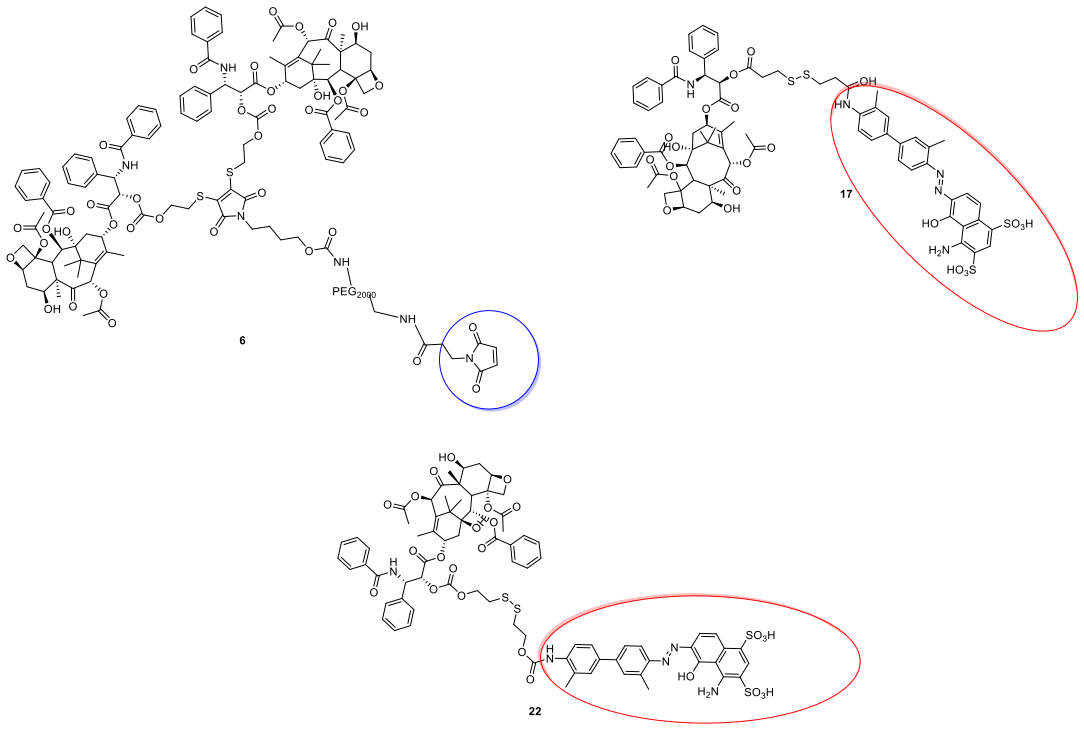

Figure 6.1

In particular, I successfully achieved the synthesis of derivatives **6**, **17** and **22** depicted above. Thanks to the presence of the terminal maleimide group, compound **6** can covalently bind HSA by reacting in situ with the SH of Cys 34. On the other side, derivatives **17** and **22** bear the tEB moiety, which is known to have high non-covalent affinity for endogenous HSA.

With this work, I paved the way to the further development of a series of chemotherapeutic prodrugs which will ultimately allow to define the best-performing chemical and physical parameters able to ensure: i) appropriate amphiphilicity to allow nanoparticles formation; ii) selectivity towards HSA; ii) ability to release the active drug under reductive TME conditions; iii) longer circulation time in the blood stream.

Our preliminary studies demonstrate that derivatives **6**, **17** and **22** possess a remarkable ability to spontaneously form nanoparticles in water with diameters in the range of 100-150 nm. Of note, preliminary stability studies in the presence of BSA at 37°C showed that nanoparticles are stable for several hours.

At present, experiments are ongoing to perform the diazotation process on compound **10** to obtain the PTX redox-responsive conjugate that eventually will be able to self-assemble into nanoparticles, ultimately providing biomimetic, bioresponsive and multi-modal delivery systems.

Future perspectives of this work include an extensive study on nanoparticles formation and characterization in terms of stability, responsiveness to redox environment through NMR and HPLC analysis and in vitro anticancer efficacy on breast cancer cells.

7. Experimental section

Materials and Methods

All commercially available reagents were used. When it was necessary the distillation of some reagent has been done. For a major part of the reactions anhydrous condition were necessary using argon or nitrogen, depending on the sensitivity of the reagent and the solvents.

MilliQ ultra-pure H2O was used for all the process which involve the use of water in the reactions or in the formation of the nanoparticles.

Characterization and purification procedure

Depending on the products obtained, different types of characterization procedure has been exploited. The progresses of reactions were followed by TLC by using aluminium and plastic-backed silica gel plates and depending on the type of compound the TLC has been burned using the Pancaldi solution or the one based on $KMnO_4$. Crude products were purified by flash chromatography (FC) using silica gel (0.037-0.063 mm, Merck) as a stationary phase. Some compounds were purified by crystallization using an appropriate solvent regulated by the solubility of the compound.

All the molecules, after the purification procedure, were characterized with Nuclear magnetic resonance spectroscopy (NMR) using a Varian MERCURY- 400 (400 MHz) spectrometer or on an Agilent NMR DD2 (500 MHz) in the stated solvents. Some crude products were purified through dialysis bag against H_2O milliQ (Tube-O-DIALYZER™, Medi, 1KDa MWCO or SnakeSkin™ Dialysis Tubing 3500 MWCO 22mm x 35 feet dry diameter).

For the filtration of the MilliQ water, the PBS or BSA solution CHROMAFIL®Xtra RC-45/13, disposable syringe filters in regenerated cellulose (0.45 µm, 13mm) were used.

For the characterization of the nanoparticles, it was performed the dynamic light scattering (DLS) to determine the hydrodynamic diameter and the polydispersity index (PDI) in aqueous solutions at 25 ◦C using a NanoBrook Omni Particle Size Analyzer (Brookhaven Instruments Corporation, USA) equipped with a 35 mW red diode laser (nominal wavelength 640 nm).

*Synthesis and characterization of compound **1***

The synthesis of this compound was carried out following a literature procedure [20]. *p*-nitrophenyl chloroformate (3.10 g, 15.4 mmol, **3eq**) and N,N-diisopropylethylamine (3,05 mL, 17.5 mmol, **2.5eq**) were added dropwise to a solution of bis(2-hydroxyethyl)disulfide (1.08 g, 7.0 mmol, **1eq**) in dry dichloromethane (1.14mL/mmol of alcohol). After stirring 5 h at room temperature, the reaction was transferred into a separatory funnel, washed with hydrochloric acid 0,1 N, saturated aqueous $NaHCO_3$ and brine. The organic layer (DCM) was dried over anhydrous Na_2SO4, filtered, and evaporated under vacuum. The crude residue was purified by flash column chromatography on silica gel (Cyclohexane(Cy) : ethyl acetate (EA)= 4:2) to afford compound **1** (scheme 19) in 80% yield.

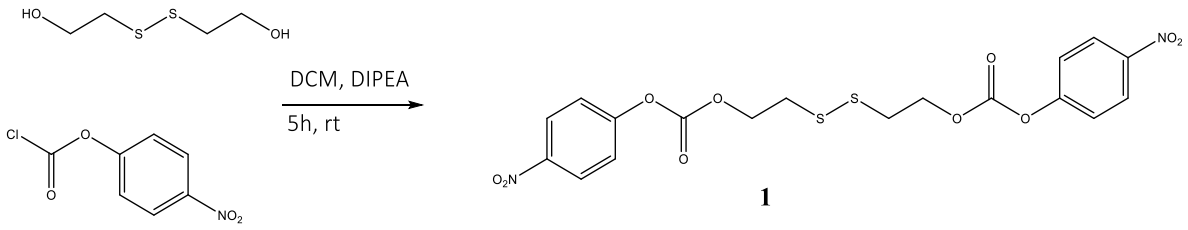

Scheme 19

After the separation on silica, compound **1** was analysed by ^{1}HNMR and compared with literature data [20].

^{1}H NMR (400 MHz; Chloroform-*d*): δ 8.28 (d, *J* = 9.2 Hz, 4H), 7.39 (d, *J* = 9.2 Hz, 4H), 4.57 (t, *J* = 6.5 Hz, 4H), 3.08 (t, *J* = 6.4 Hz, 4H).

Synthesis and characterization of compound **3**

Compound **3** was obtained through a two-step procedure according to literature reports[29].

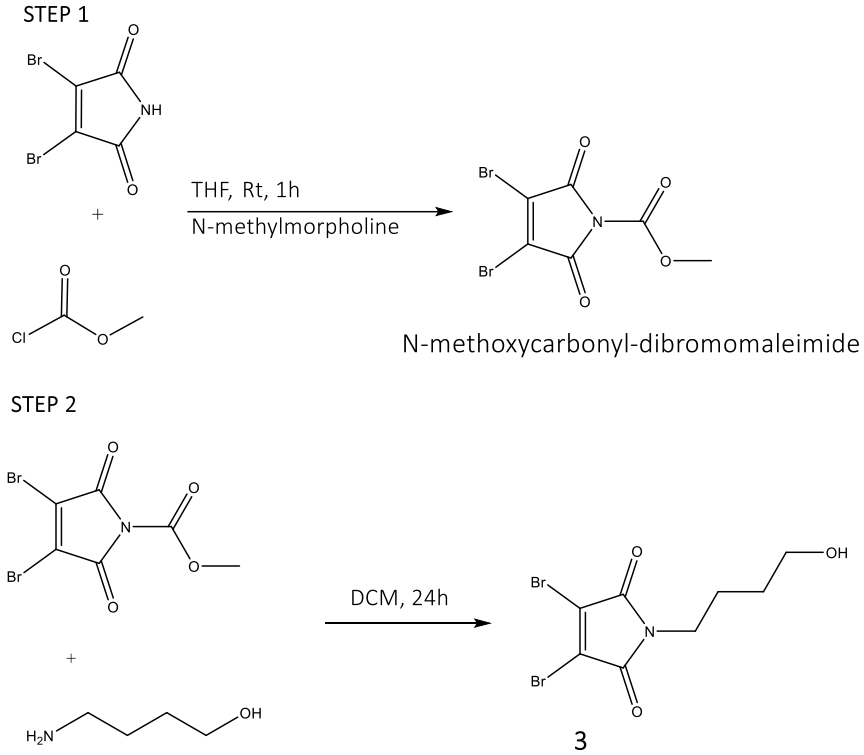

Scheme 20

STEP 1

3,4-dibromomaleimide (300 mg, 1,18 mmol, **1eq**) (scheme 20) was dissolved in anhydrous THF (10,6ml) followed by sequential addition of N-methyl morpholine (119 mg, 1,18 mmol, **1eq**) and methyl chloroformate (111.51 mg, 1,18 mmol, **1eq**). The mixture was stirred for 1 h at room temperature. When methyl-chloroformate is added, the solution color suddenly turns to bright pink (figure 7.1).


Figure 7.1 Photos of the particular colour obtained during the synthesis of N-methoxycarbonyl-dibromomaleimide

After 1 h at room temperature, THF was removed under vacuum and the crude product was dissolved in DCM and washed with HCl 0,1 N and two times with brine. Then the organic phase was dried over Na_2SO_4 and the solvent removed in vacuo to yield compound N-methoxycarbonyl-dibromomaleimide as a pink powder (Y = 80%).

^{1}H NMR (400 MHz; Chloroform-*d*): δ 4 (s, 3H)

STEP 2

N-methoxycarbonyl-dibromomaleimide (175,5 mg, 0.561 mmol, **1eq**) (scheme 20) was dissolved in dichloromethane (20,9 mL) and then 4-amino-1-buthanol (50 mg, 0.561 mmol, **1eq**) was added to the stirring solution. The colour changes rapidly also during this reaction, starting from a pale orange to reach a dark orange (figure 7.2).


Figure 7.2 Photos of the solution colour obtained in the STEP 2 of the synthesis of of compound 3

After 24 h the mixture was concentrated to dryness and the crude residue was purified by column chromatography (3:2 =Cy/EA) to yield compound **3** as a pale-yellow solid (Y = 60%). Then the ^{1}HNMR spectra of the compound in $CDCl_3$ was investigated confirming literature data.

^{1}H NMR (400 MHz; Chloroform-*d*): δ 3.67 (m, 4H), δ 1.72 (m, 2H) and δ=1.57 (m, 2H)

*Synthesis and characterization of compound **2***

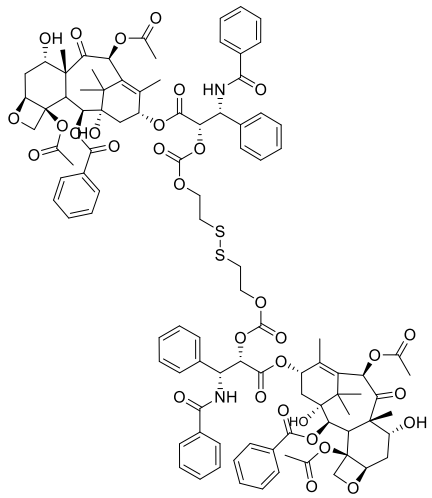

2

Figure 7.3

The synthesis of compound **2** (figure 7.3) was achieved following a literature procedure [20]. Compound **1** (38.36 mg, 0.084 mmol, **1eq**) was dissolved in DCM (1.53 mL), then 7-epi-PTX (150 mg, 0.176 mmol, **2.09eq**) and an excess of DMAP (22.37 mg, 0.183 mmol, **2.18eq**) were added. After a night at room temperature, the crude reaction mixture was washed using HCl 0.1 N, saturated $NaHCO_3$ and brine. Then the organic phase was dried over Na_2SO_4 and isolated by flash column chromatography (EA : Cy = 1:1) yield as a white solid (Y = 83%).

^{1}H NMR (400 MHz, $CDCl_3$) δ 8.18 (dd, *J* = 8.4, 1.3 Hz, 7H), 7.75 – 7.67 (m, 7H), 7.64 – 7.30 (m, 31H), 7.03 – 6.97 (m, 2H), 6.82 (d, *J* = 3.1 Hz, 4H), 6.26 (d, *J* = 7.2 Hz, 2H), 6.03 (dd, *J* = 9.5, 2.8 Hz, 2H), 5.76 (dd, *J* = 7.4, 2.7 Hz, 3H), 5.47 (dd, *J* = 5.7, 2.9 Hz, 4H), 4.94 (dd, *J* = 9.1, 3.6 Hz, 3H), 4.49 (td, J = 6.5, 1.9 Hz, 2H), 4.39 (d, *J* = 3.1 Hz, 5H), 4.34 (td, *J* = 6.6, 3.3 Hz, 3H), 3.93 (dd, *J* = 7.5, 4.0 Hz, 3H), 3.51 – 3.44 (m, 1H), 3.34 (t, *J* = 6.3 Hz, 2H), 2.86 (t, *J* = 6.6 Hz, 4H), 2.61 – 2.50 (m, 9H), 2.47 – 2.23 (m, 6H), 2.22 – 2.09 (m, 14H), 1.90 (dd, *J* = 4.0, 1.4 Hz, 8H), 1.67 (d, *J* = 3.1 Hz, 8H), 1.59 (s, 4H), 1.26 – 1.11 (m, 15H).

*Synthesis and characterization of compound **4***

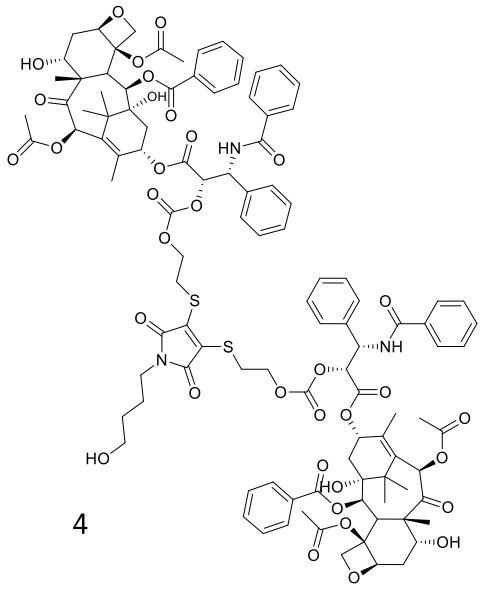

Figure 7.4

The synthesis of compound **4** (figure 7.4) was achieved following a slightly modified literature procedure in order to enhance the reaction yield [23]. In a round bottom flask, the dimer of 7-epi-PTX (**2**) (60 mg, 0.031 mmol, **1eq**) was dissolved in anhydrous THF (1 mL), then compound **3** (9.12 mg, 0.028 mmol, **0.8eq**) was added to the stirred solution. After that, 1 mL of anhydrous MeOH and tris(2-carboxyethyl)phosphine(TCEP) (17 mg, 0.060 mmol, **2.8eq**) were added to the mixture. After the dissolution of TCEP, TEA (20 µL, 0.086 mmol, **1eq**) was added dropwise and the reaction was left reacting at room temperature overnight. The reaction mixture was washed with HCl 0.1N and saturated NH_4Cl; the organic layer was then dried over Na_2SO_4 and the desired product was isolated by flash column chromatography (Cy: EA = 1:3) (Y =20%). The same reaction was performed starting from paclitaxel and the herein reported procedure was optimized obtaining a higher yield.

^{1}H NMR (400 MHz, CDCl3) δ 8.19 (ddd, *J* = 6.8, 5.2, 1.2 Hz, 4H), 7.76 – 7.69 (m, 3H), 7.63 – 7.29 (m, 18H), 7.08 (d, *J* = 9.4 Hz, 1H), 6.84 – 6.78 (m, 2H), 6.23 (d, *J* = 3.8 Hz, 1H), 6.02 (dd, *J* = 9.5, 3.0 Hz, 1H), 5.76 (d, *J* = 7.4 Hz, 1H), 5.48 – 5.41 (m, 2H), 4.97 – 4.89 (m, 1H), 4.44 – 4.31 (m, 4H), 4.30 – 4.22 (m, 1H), 3.97 – 3.88 (m, 2H), 3.58 – 3.39 (m, 5H), 3.09 (s, 1H), 2.62 – 2.52 (m, 6H), 2.39 (d, *J* = 9.6 Hz, 2H), 2.29 (s, 2H), 2.23 – 2.13 (m, 8H), 2.07 – 2.00 (m, 9H), 1.94 – 1.85 (m, 5H), 1.70 – 1.64 (m, 5H), 1.42 (s, 1H), 1.19 (ddd, *J* = 18.2, 16.6, 10.7 Hz, 10H), 0.07 (s, 2H).

*Synthesis and characterization of compound **5***

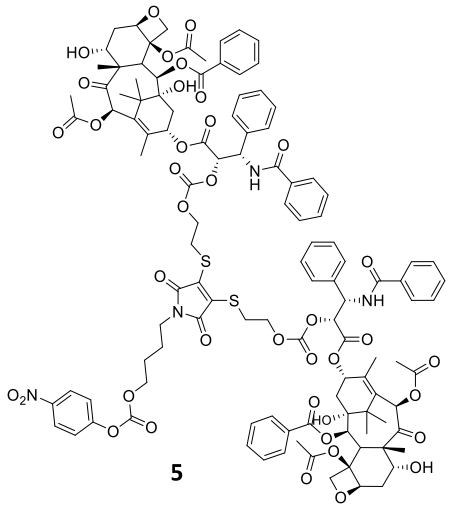

Figure 7.5

Compound **4** (20 mg, 0.01 mmol, **1eq**) was dissolved in anhydrous DCM (900 µL), followed by sequential addition of DMAP (0.120 mg, 0.001 mmol, **0.1eq**) and TEA (1.36 µL, 0.01 mmol, **1eq**). Next, 4-nitrophenyl chloroformate (5.65 mg, 0.027 mmol, **2.86eq**) was dissolved in the solution and the reaction was left at room temperature for 5 h. For the workout, the mixture was washed using HCl 0.1 N, $NaHCO_3$ and Brine, then the organic phase was dried over Na_2SO_4 and the crude (figure 7.5) was purified by flash column chromatography (Cy : EA = 2:3) to obtain the desired compound (Y = 40%).

^{1}H NMR (400 MHz, $CDCl_3$) δ 8.21 – 8.15 (m, 4H), 8.11 (d, *J* = 9.2 Hz, 1H), 7.78 – 7.68 (m, 4H), 7.68 – 7.30 (m, 22H), 7.05 (d, *J* = 9.6 Hz, 1H), 6.88 – 6.78 (m, 4H), 6.23 (s, 2H), 6.03 (dd, *J* = 9.4, 2.9 Hz, 2H), 5.76 (dd, *J* = 7.6, 2.7 Hz, 3H), 5.50 – 5.41 (m, 3H), 5.06 – 4.88 (m, 2H), 4.78 – 4.64 (m, 2H), 4.37 (dd, *J* = 13.3, 9.5 Hz, 6H), 4.31 – 4.23 (m, 2H), 3.96 – 3.88 (m, 2H), 3.68 (s, 2H), 3.53 – 3.42 (m, 2H), 3.11 (s, 1H), 2.56 (dt, *J* = 8.2, 5.0 Hz, 8H), 2.27 – 2.09 (m, 12H), 1.94 – 1.86 (m, 7H), 1.77 – 1.49 (m, 16H), 1.22 – 1.09 (m, 11H).

*Synthesis and characterization of compound **6***

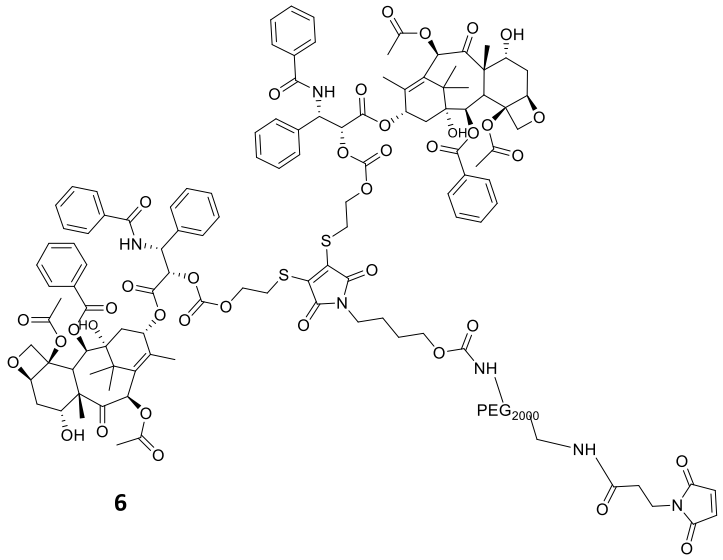

6

Figure 7.6

Compound **5** (8.7 mg, $3.9 \cdot 10^{-3}$mmol, **1eq**) was dissolved in 1 mL of anhydrous DCM then TEA (1.52 µL, 0.0109mmol, **2.8eq**) was added dropwise to the solution; next, MAL-PEG-$NH_3^+TFA^-$ (10.48mg, 0.0054mmol, **1.4eq**) dissolved in 1mL of DCM was added. After a night at room temperature the reaction mixture was washed with EA and water to remove the un-reacted PEGylated derivative. The crude product was transferred into a dialysis bag (SnakeSkin dialysis tubing 3500 MWCO) and purified against water/DMSO (3%) by changing the external medium every 2h for 24h allowing to isolate the pure compound in 90% yield (figure 7.6).

^{1}H NMR (400 MHz, $CDCl_3$ δ 8.18 (d, *J* = 7.0, 1.8 Hz, 1H), 7.86 – 7.73 (m, 1H), 7.71 (d, 1H), 7.64 – 7.30 (m, 17H), 7.06 – 6.98 (m, 1H), 6.81 (d, *J* = 2.1 Hz, 2H), 6.29 – 6.20 (m, 2H), 6.02 (dd, *J* = 9.7, 3.0 Hz, 1H), 5.75 (d, *J* = 7.0 Hz, 2H), 5.49 – 5.41 (m, *J* = 5.5, 2.9 Hz, 2H), 4.92 (dd, *J* = 9.2, 5.3 Hz, 3H), 4.70 (dd, *J* = 14.3, 5.8 Hz, 2H), 4.45 – 4.30 (m, 6H), 3.92 (dt, *J* = 11.5, 4.2 Hz, 4H), 3.87 – 3.32 (m, 374H), 2.86 (t, *J* = 6.5 Hz, 1H), 2.58 – 2.51 (m, 6H), 2.21 – 2.14 (m, 8H), 1.90 (t, *J* = 3.9 Hz, 5H), 1.68 (t, *J* = 7.3 Hz, 7H), 1.41 (d, *J* = 5.7 Hz, 1H), 1.15 (dd, *J* = 10.3, 2.7 Hz, 9H).

*Synthesis and characterization of compound **7***

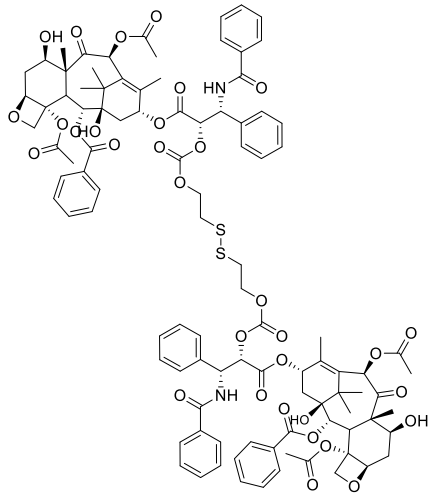

7

Figure 7.7

The synthesis of the PTX-SS-PTX dimer carbonate was achieved following a literature procedure [20]. Compound **1** (38.4 mg, 0.084 mmol, **1eq**) was dissolved in DCM (1.53 mL), then PTX (150 mg, 0.176 mmol, **2.09eq**) and an excess of DMAP (22.37 mg, 0.183 mmol, **2.18eq**) were added. After a night at room temperature, the crude reaction mixture was washed with HCl 0.1N, saturated $NaHCO_3$ and Brine. The organic phase was then dried over Na_2SO_4 and the product (figure 7.7) isolated by flash column chromatography (EA : Cy = 1:1) as a white solid (Y = 83%).

^{1}H NMR (400 MHz, $CDCl_3$) 1H NMR (400 MHz, cdcl3) δ 8.14 (d, *J* = 7.1 Hz, 4H), 7.72 (d, *J* = 7.1 Hz, 4H), 7.60 (d, *J* = 7.6 Hz, 2H), 7.55 – 7.32 (m, 10H), 6.96 (d, *J* = 9.4 Hz, 1H), 6.29 (s, 1H), 6.26 (dd, *J* = 9.2, 1.7 Hz, 1H), 6.00 (dd, *J* = 9.4, 2.9 Hz, 2H), 5.68 (d, *J* = 7.0 Hz, 1H), 5.44 (d, *J* = 2.9 Hz, 2H), 4.97 (dd, *J* = 9.8, 2.5 Hz, 2H), 4.47 – 4.28 (m, 5H), 4.20 (dd, *J* = 8.4, 0.7 Hz, 2H), 3.81 (d, *J* = 7.0 Hz, 2H), 2.88 (t, *J* = 6.5 Hz, H), 2.49 (d, *J* = 4.1 Hz, 2H), 2.46 (s, 5H), 2.41 – 2.35 (m, 1H), 2.21 (s, 8H), 2.17 (s, 1H), 1.92 (d, *J* = 1.3 Hz, 5H), 1.76 (s, 2H), 1.68 (s, 4H), 1.61 (s, 9H), 1.27 (s, 3H), 1.23 (s, 5H), 1.13 (s, 3H)

*Synthesis and characterization of compound **8***

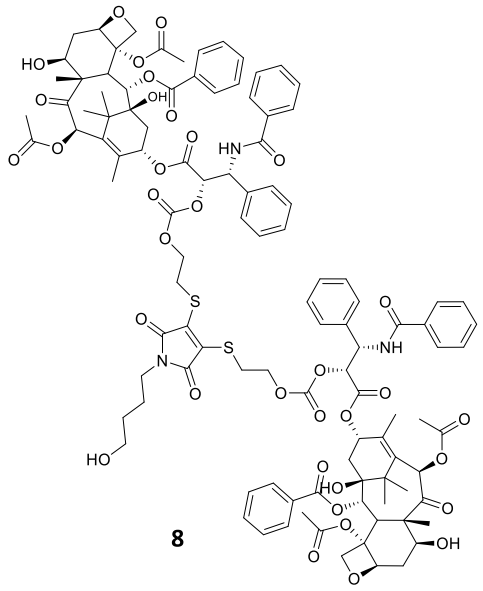

Figure 7.8

The synthesis of compound **8** was achieved following a slightly modified literature procedure enhance the reaction yield [23]. In a round bottom flask, the dimer of PTX (**7**) (150 mg, 0.078 mmol, **1eq**) was dissolved in anhydrous THF (1 mL), then compound **3** (28 mg, 0.09 mmol, **1.1eq**) was added to the stirred solution. When all compounds were completely dissolved, MeOH (4 mL anhydrous) and tris(2-carboxyethyl)phosphine(TCEP) (40.21 mg, 0.14 mmol, **1.8eq**) were inserted in the flask. After the dissolution of TCEP, DIPEA (68.43 µL, 0.392 mmol, **5eq**) was added drop by drop and the reaction was left for 15 minutes at room temperature. The colour of the solution changed from a pale yellow to a strong fluo yellow (**figure 7.9**), during DIPEA addition.

Figure 7.9** Photo of the crude mixture with compound **8

The crude reaction mixture (figure 7.9) was then washed with HCl 0.1N and saturated NH_4Cl, and the organic solution was dried over Na_2SO_4 and isolated by flash column chromatography (DCM: EA = 1:3) with a yield of 60%.

^{1}H NMR (400 MHz, $CDCl_3$) δ 8.14 (d, *J* = 7.0 Hz, 4H), 7.74 (d, *J* = 7.2 Hz, 4H), 7.65 – 7.56 (m, 2H), 7.56 – 7.34 (m, 15H), 7.02 (d, *J* = 9.4 Hz, 2H), 6.29 (s, 1H), 6.24 (t, *J* = 4.6 Hz, 2H), 5.99 (dd, *J* = 9.3, 3.0 Hz, 2H), 5.69 (d, *J* = 7.0 Hz, 2H), 5.43 (d, *J* = 2.9 Hz, 2H), 4.97 (dd, *J* = 9.6, 2.4 Hz, 2H), 4.48 – 4.25 (m, 6H), 4.20 (d, *J* = 8.4 Hz, 2H), 3.80 (d, *J* = 7.2 Hz, 2H), 3.61 – 3.39 (m, 6H), 2.63 (d, *J* = 4.3 Hz, 2H), 2.44 (s, 6H), 2.37 (d, *J* = 9.2 Hz, 1H), 2.22 (d, *J* = 9.2 Hz, 7H), 1.92 – 1.86 (m, 7H), 1.69 (d, *J* = 3.9 Hz, 5H), 1.55 – 1.38 (m, 2H), 1.23 (s, 5H), 1.14 (s, 4H).

*Synthesis and characterization of compound **9***

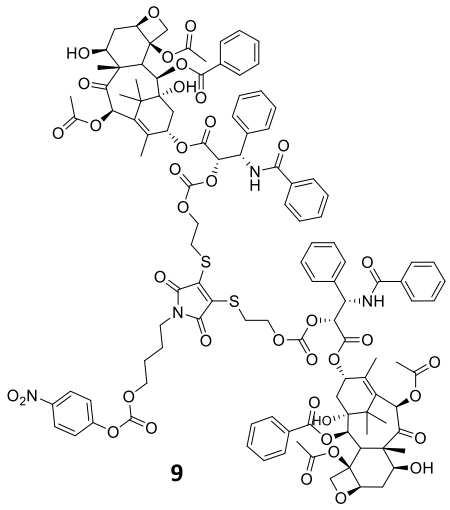

9

Figure 7.10

Compound **8** (85.2 mg, 0.048 mmol, **1eq**) (figure 7.10) was dissolved in anhydrous DCM (2 mL), then DMAP (3.99 mg, 0.0327 mmol, **0.8eq**) and TEA (5.68 µL, 0.0408 mmol, **1eq**) were added. Next, 4-nitrophenyl chloroformate (20.58 mg, 0.102 mmol, **2.5eq**) was dissolved in the solution and the reaction was left at room temperature for 5 hours. The mixture was then washed with HCl 0.1 N, $NaHCO_3$ and Brine, and the organic phase was dried over Na_2SO_4. The crude product (figure 7.11) was purified by flash column chromatography (Cy : EA= 2:3) to obtain the desired compound (Y = 47%).

^{1}H NMR (400 MHz, CDCl3) δ 8.25 (d, *J* = 9.2 Hz, 4H), 8.14 (d, *J* = 7.1 Hz, 7H), 7.78 – 7.70 (m, 7H), 7.65 – 7.56 (m, 4H), 7.51 (dd, *J* = 9.8, 8.3 Hz, 9H), 7.45 – 7.26 (m, 24H), 6.99 (d, *J* = 9.4 Hz, 3H), 6.29 (s, 3H), 6.25 (dd, *J* = 6.2, 4.4 Hz, 2H), 6.00 (dd, *J* = 9.4, 2.9 Hz, 3H), 5.68 (d, *J* = 7.0 Hz, 3H), 5.43 (d, *J* = 2.9 Hz, 4H), 4.97 (dd, *J* = 9.7, 2.6 Hz, 3H), 4.47 – 4.22 (m, 2H), 4.20 (d, *J* = 8.2 Hz, 3H), 3.80 (d, *J* = 7.0 Hz, 3H),

3.50 (ddd, *J* = 14.3, 6.9, 3.5 Hz, 5H), 2.50 (d, *J* = 4.1 Hz, 2H), 2.45 (s, 9H), 2.21 (d, *J* = 2.7 Hz, 14H), 1.90 (d, *J* = 1.5 Hz, 10H), 1.84 (s, 3H), 1.68 (t, *J* = 3.2 Hz, 11H), 1.61 (s, 11H), 1.22 (s, 8H), 1.13 (s, 7H).

*Synthesis and characterization of compound **10***

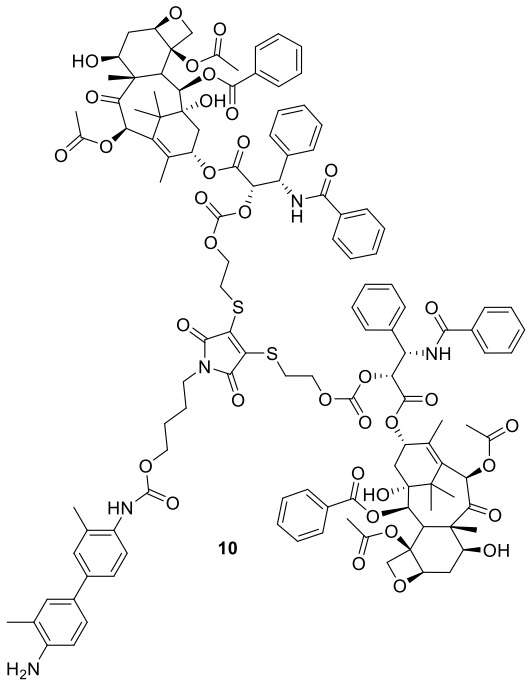

Figure 7.11

The reaction was carried out under anhydrous conditions at room temperature for a night. At first hydroxybenzotriazole (HOBt 2.86 mg, 0.021 mmol, **1eq**) was dissolved in 425 µL of dry DMF (with MS 4 Å). Then o-tolidine (5.53 mg, 0.026 mmol, **1.5eq**) and compound **9** (39 mg, 0.017 mmol, **1eq**) were added. After a night, the solvent was removed using under high vacuum and the dried crude mixture was washed and filtered with EA. The product (figure 7.11) was purified by flash column chromatography (Cy : EA = 1:2) with a yield of 48%. The presence of o-tolidine in TLC was pointed out using a cerium molibdate stain solution through the formation of a greenish spot.

^{1}H NMR (400 MHz, cdcl$_3$) δ 8.19 – 8.10 (m, 4H), 7.77 – 7.70 (m, 4H), 7.63 – 7.30 (m, 22H), 7.05 – 6.97 (m, 2H), 6.71 (dd, *J* = 8.0, 3.0 Hz, 1H), 6.31 – 6.18 (m, 3H), 5.99 (dd, *J* = 9.3, 2.8 Hz, 2H), 5.68 (d, *J* = 7.2 Hz, 2H), 5.43 (d, *J* = 2.9 Hz, 2H), 4.97 (dd, *J* = 9.7, 2.4 Hz, 2H), 4.47 – 4.24 (m, 5H), 4.22 – 4.16 (m, 2H), 3.80 (d, *J* = 7.6 Hz, 2H), 3.47 (dt, *J* = 11.9, 5.5 Hz, 3H), 2.55 (ddd, *J* = 14.5, 9.5, 6.5 Hz, 2H), 2.49 – 2.33 (m, 7H), 2.31 – 2.14 (m, 15H), 2.04 (d, *J* = 3.5 Hz, 6H), 1.95 – 1.81 (m, 7H), 1.68 (s, 4H), 1.61 (d, *J* = 11.0 Hz, 9H), 1.29 – 1.19 (m, 7H), 1.13 (s, 3H).

Nanoparticles preparation

In a vial, 15 mg of the *compound* ***6*** were dissolved in 1 mL of dimethyl sulfoxide (DMSO). After complete dissolution, 67 µL of this solution were added dropwise via syringe and under vigorous stirring to a second vial containing ultrapure H_2O (filtered on 0.45 µm), in order to reach 1 mg/mL concentration. After some minutes of stirring, half of the solution was taken and inserted in a cuvette previously filled with 1,2 mL of filtered PBS (pH =7.4, 10mM).

Synthesis and characterization of compound **11**

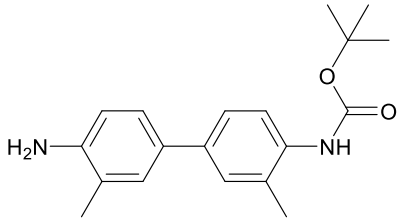

11

Figure 7.12

In a round bottom flask, o-tolidine (1.06g, 5mmol, **1eq**) was dissolved in anhydrous DCM (10mL) under stirring. After the complete dissolution, BOC_2O (1.09g, 5mmol, **1eq**) was added to the solution and the reaction mixture was left for 24h under stirring at room temperature. The crude product was then purified through flash column chromatography (Cy:EA = 2:1) leading to **11** with a yield of 67%. The purified compound **11** (figure 7.12) was then analysed at ^{1}HNMR in $CDCl_3$.

^{1}H NMR (500 MHz, $CDCl_3$) δ 7.80 (d, *J* = 6.1 Hz, 1H), 7.51 – 7.20 (m, 4H), 6.75 (d, *J* = 8.0 Hz, 1H), 6.26 (s, 1H), 3.84 (s, 2H), 2.35 – 2.19 (m, 6H), 1.54 (s, 9H), 1.42 (d, *J* = 11.9 Hz, 1H).

Synthesis and characterization of compound **12**

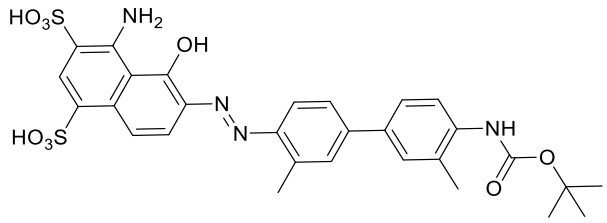

12

Figure 7.13

The diazotation procedure is divided into 3 Steps:

STEP 1

In a vial, compound **11** (150 mg, 0.48 mmol, **1eq**) was dissolved in 3.3mL of acetonitrile at 0°C. When everything was dissolved, two solutions were added, previously cooled down at 0°C, the first one was HCl 0.3 N (4.9 mL) and, after few minutes, the second one, a solution of $NaNO_2$ (100.7 mg, 1.44 mmol, **3eq**, dissolved in 4 mL of MilliQ H_2O). The reaction mixture colour change from pink to a cadmium yellow. Then the reaction was left a 0°C for 30 minutes.

STEP 2

In another vial, 1-amin-8-naphtol-2,4-disulfonic acid was added to a stirred solution of sodium bicarbonate (145.16 mg, 1.73 mmol, **3.6eq**) dissolved in 1 mL of ultrapure water at 0°C.

STEP 3

After 30 min the solution obtained in step 1 was transferred into the step 2 vial. The colour immediately turned to dark violet, and the mixture was left stirring at 10°C for 3 h.

To remove water and acetonitrile, the mixture was then lyophilized. The dry powder was then dissolved in a little amount of water and MeOH and transferred into a dialysis against water. The external medium was changed every 8 h (3 times) and replenished with fresh one to remove the salts that were formed during the reaction (Y = 57.5 %). The product (figure 7.13) was then analysed by ^{1}H NMR spectroscopy.

^{1}H NMR (500 MHz, DMSO) δ 8.59 – 8.40 (m, 1H), 8.03 (s, 1H), 7.60 – 7.38 (m, 2H), 7.32 (s, 1H), 7.27 (s, 1H), 7.23 – 7.13 (m, 1H), 7.06 – 6.88 (m, 1H), 6.64 (d, *J* = 8.1 Hz, 1H), 4.91 (s, 1H), 3.15 (s, 7H), 2.65 (d, *J* = 26.4 Hz, 1H), 2.28 – 2.23 (m, 2H), 2.20 (s, 2H), 2.08 (d, *J* = 10.3 Hz, 2H), 1.46 (d, *J* = 8.8 Hz, 9H).

*Synthesis and characterization of compound **13***

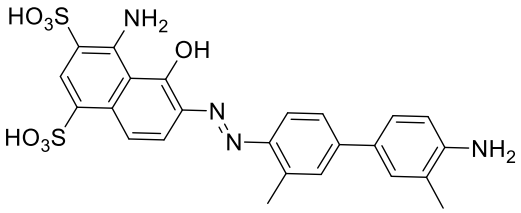

13

Figure 7.14

Compound **12** (150mg, 0.23mmol, **1eq**) was dissolved in water and inserted into a microwave apparatus at 300 W with an internal pressure of 5 Bar for 8 min [24]; tEB (**13**) (figure 7.14) was obtained in quantitative yield as pure dark red powder upon freeze drying.

^{1}H NMR (400 MHz, CD_3OD) δ 8.70 (s, 1H), 7.98 (d, *J* = 9.8 Hz, 1H), 7.90 (d, *J* = 8.6 Hz, 1H), 7.50 (dt, *J* = 17.8, 2.5 Hz, 2H), 7.34 – 7.24 (m, 2H), 7.17 (d, *J* = 10.0 Hz, 1H), 6.76 (d, *J* = 8.2 Hz, 1H), 2.52 (s, 3H), 2.21 (s, 4H).

*Synthesis and characterization of compound **14***

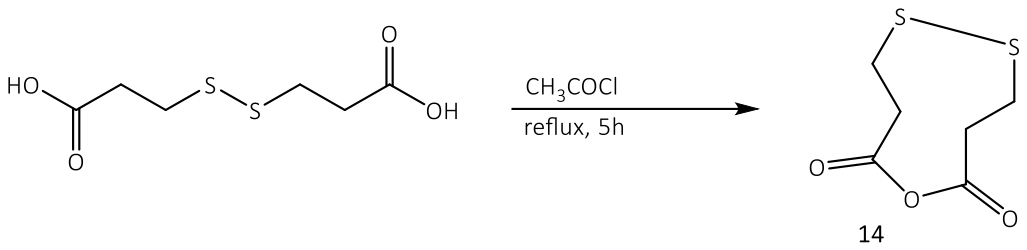

14

Scheme 21

In a round bottom flask, 15 mL of acetyl chloride (2.08 g; 9.6 mmol, **1eq**) and 3,3'-disulfanediyldipropionic acid (15mL, 1.56mL/mmol CH_3COCl) were added (scheme 21). The reaction was carried out under reflux (51°C) for 5 h. The mixture was then washed with toluene and the solvent removed with high vacuum rotary evaporator. To promote the precipitation of the anhydride as a crystalline solid, the obtained material was dissolved in toluene and Et_2O was added (1:2) and at 0°C to allow the precipitation. Finally, all solvents were removed and the solid under vacuum.

^{1}H NMR (400 MHz, DMSO) δ 2.86 (t, *J* = 6.9 Hz, 4H), 2.60 (t, *J* = 6.9 Hz, 4H).

Synthesis and characterization of compound **15**

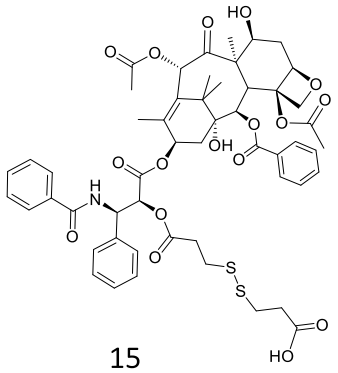

15

Figure 7.15

Compound **14** (80.95 mg, 0.234 mmol, **1.8eq**) was dissolved in anhydrous DCM then TEA (97.58µL, 0.702mmol, **3eq**) was dripped inside the flask obtaining a pale-yellow colour.

When everything was dissolved 7-epi-PTX (200mg, 0.234 mmol, **1eq**) was added to the reaction mixture and left overnight under inert atmosphere. The solution was then washed with HCl 0.1N and Brine and the organic phase was dried over Na_2SO_4. Then the crude product (figure 7.15) was purified on silica gel flash column chromatography (DCM : MeOH = 10:1) to afford the desired compound in 77% yield.

^{1}H NMR (400 MHz, $CDCl_3$) δ 8.17 (dd, *J* = 7.0, 1.7 Hz, 2H), 7.74 (dd, *J* = 7.0, 1.7 Hz, 2H), 7.64 – 7.30 (m, 9H), 7.23 (s, 1H), 6.81 (s, 1H), 6.22 (td, *J* = 9.1, 1.7 Hz, 1H), 6.03 (dd, *J* = 9.4, 3.5 Hz, 1H), 5.76 (d, *J* = 7.4 Hz, 1H), 5.59 (d, *J* = 3.5 Hz, 1H), 4.94 (dd, *J* = 9.2, 3.5 Hz, 1H), 4.68 (d, *J* = 11.4 Hz, 1H), 4.51 – 4.28 (m, 2H), 3.93 (d, *J* = 7.4 Hz, 1H), 3.78 – 3.66 (m, 1H), 3.01 – 2.58 (m, 11H), 2.57 (s, 2H), 2.44 – 2.24 (m, 2H), 2.24 – 2.14 (m, 4H), 1.90 (d, *J* = 1.5 Hz, 2H), 1.66 (s, 2H), 1.16 (d, *J* = 11.9 Hz, 4H).

*Synthesis and characterization of compound **16***

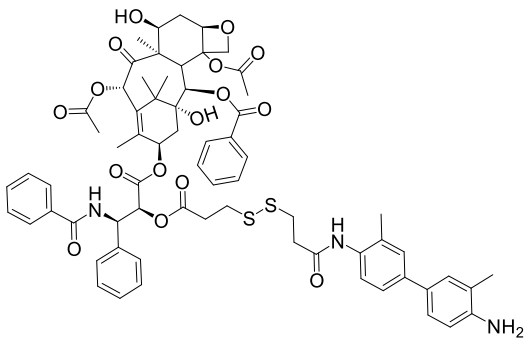

16

Figure 7.16

The synthesis of compound **16** (figure 7.16) was carried out following a literature procedure [26]. Compound **15** (38.7mg, 0.037 mmol, **1eq**) was dissolved in anhydrous THF (1 mL), then o-tolidine (9.42 mg, 0.044 mmol, **1.2eq**) was added to the stirred solution. After the dissolution, PyBOP (31.13mg, 0.059 mmol, **1.6eq**) and DIPEA (64.65µL, 0.37 mmol, **10 eq**) were added dropwise. After 1 hour and half, the solution was diluted with EA and washed with distilled water. The organic layer was dried over Na_2SO_4.

The product was isolated by silica gel flash column chromatography (EA : Cy = 5:2) (Y = 32%). The presence of o-tolidine in TLC was pointed out using a cerium molibdate stain solution through the formation of a greenish spot.

^{1}H NMR (400 MHz, Acetone) δ 8.13 (dd, *J* = 7.1, 1.4 Hz, 2H), 7.74 (dd, 2H), 7.69 (d, *J* = 9.2 Hz, 1H), 7.63 – 7.20 (m, 21H), 6.81 (s, 1H), 6.77 (d, *J* = 8.0 Hz, 1H), 6.14 (s, 1H), 5.96 (dd, *J* = 9.3, 4.6 Hz, 1H), 5.72 (d, *J* = 7.6 Hz, 1H), 5.55 (d, *J* = 4.7 Hz, 1H), 4.89 (dd, J = 8.9, 3.8 Hz, 1H), 4.67 (d, *J* = 11.5 Hz, 1H), 4.36 (s, 2H), 3.89 (d, *J* = 7.6 Hz, 1H), 3.71 – 3.64 (m, 1H), 3.03 – 2.82 (m, 4H), 2.70 (ddd, *J* = 21.5, 15.0, 8.1 Hz, 1H), 2.45 (s, 2H), 2.36 – 2.19 (m, 9H), 1.93 – 1.84 (m, 4H), 1.69 – 1.60 (m, 3H), 1.26 (s, 1H), 1.13 (d, *J* = 7.6 Hz, 5H).

*Synthesis and characterization of compound **17***

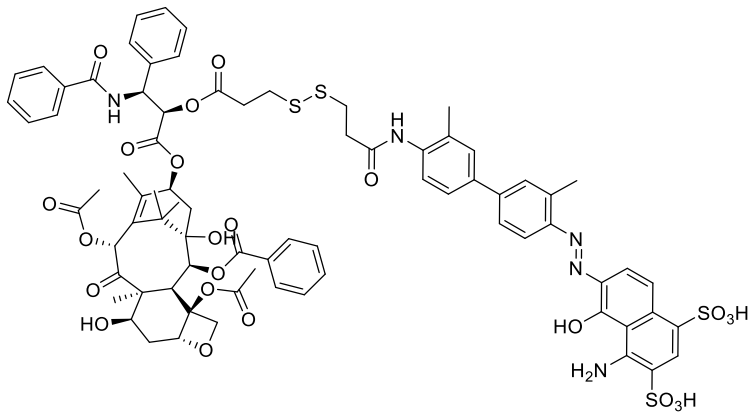

17

Figure 7.18

The diazotation procedure is divided into 3 Steps:

STEP 1

In a vial, compound **16** (41.7 mg, 0.0332mmol, **1eq**) was dissolved in 678µL of acetonitrile at 0°C. When everything was dissolved, two solutions previously cooled down at 0°C were added, the first

one was HCl 0.3 N (339 µL) and, after few minutes, the second one, a solution of $NaNO_2$(6.87 mg, 0.099 mmol, **3eq**, dissolved in 395 µL of MilliQ H_2O). The color change from pink to a cadmium yellow. Then the reaction was left a 0°C for 30 minutes.

STEP 2

In a second vial, at 0°C, sodium bicarbonate (10.04 mg, 0.120 mmol, **3.6eq**) was dissolved in 395 µL of MilliQ H_2O; subsequently 1-amin-8-naphtol-2,4-disulfonic acid was added to this stirred solution.

STEP 3

After the half hour the solution inside the vial of the step 1 was transferred in the solution of the vial of the step 2. The colour changed completely and became violet. Then the reaction was left for 3 hours at 10° C.

To remove water and acetonitrile, the mixture was then lyophilized. The obtained solid crude product was then dissolved in a little amount of water and DMSO and the solution was put in dialysis to remove the salts that were formed during the diazotation process (Y = 57.5 %).

^{1}H NMR (400 MHz, DMSO) δ 9.41 (s, 1H), 9.20 (d, *J* = 8.6 Hz, 1H), 8.44 (s, 1H), 8.35 (s, 1H), 8.11 (s, 1H), 7.99 (ddd, *J* = 9.8, 6.9, 5.7 Hz, 6H), 7.92 – 7.79 (m, 5H), 7.79 – 7.59 (m, 8H), 7.59 – 7.35 (m, 16H), 7.19 – 7.10 (m, 2H), 6.98 (d, *J* = 10.0 Hz, 1H), 6.62 (d, *J* = 2.5 Hz, 2H), 5.81 (d, *J* = 10.8 Hz, 2H), 5.56 (t, *J* = 8.7 Hz, 2H), 5.47 (d, *J* = 7.4 Hz, 2H), 5.38 (d, *J* = 8.8 Hz, 2H), 4.95 (dt, *J* = 11.9, 3.2 Hz, 3H), 4.66 (s, 2H), 4.24 (d, *J* = 8.6 Hz, 2H), 4.12 (d, *J* = 8.2 Hz, 2H), 3.68 (d, *J* = 7.4 Hz, 2H), 3.55 – 3.40 (m, 2H), 2.95 (dd, *J* = 12.9, 6.0 Hz, 2H), 2.86 (dd, *J* = 20.3, 14.3 Hz, 3H), 2.67 (dd, *J* = 14.7, 12.8 Hz, 2H, 2.14 – 1.94 (m, 11H), 1.91 – 1.81 (m, 1H), 1.66 (d, *J* = 1.2 Hz, 4H), 1.50 (s, 5H), 1.21 (s, 1H), 0.98 (t, *J* = 6.4 Hz, 8H).

Nanoprecipitation method

In a vial, 4 mg of *compound **17*** was dissolved in 1 mL of ethanol under stirring and sonication. Afterwards, the solution was filtered on cotton to remove residual undissolved compound. 395 µL of this clear solution (3.5 mg/mL) was added to a vial containing MilliQ H_2O (filtered on 0.45 µm syringe filters) under vigorous stirring to reach a final concentration of 1.5 mg/mL. The same procedure was applied to compound EpiPTX (**22**). After some minutes of stirring, half of the solution was taken and inserted in a cuvette previously filled with 1mL of filtered H_2O or with 1mL of filtered BSA solution (30mg/mL) in order to have a final volume of 1.8 mL and a concentration of 0.4 mg/mL. The analysis was performed by DLS giving the results shown in paragraph 5.5.2.

*Synthesis and characterization of compound **20***

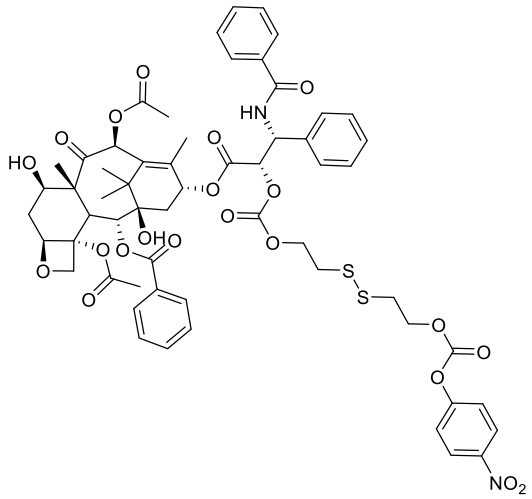

20

Figure 7.19

In a round-bottomed flask, compound **1** (100.9mg, 0.221mmol,**1.3eq**) was dissolved in 3 mL of anhydrous DCM, and, after the dissolution, PTX (150 mg, 0.17 mmol, **1eq**) and a sub-catalytic amount of DMAP (45.27 mg, 0.370 mmol, **0.6eq**) were added. After 5 hours at room temperature, the mixture was washed with HCl 0.1 N and Brine. Then the organic phase was dried over Na_2SO_4 and the crude product (figure 7.19) was purified by silica gel flash column chromatography (EA: DCM = 1:1) (Y: 54%). ^{1}H NMR (400 MHz, $CDCl_3$) δ 8.26 – 8.20 (m, 2H), 8.18 – 8.11 (m, 2H), 7.75 – 7.68 (m, 2H), 7.60 (ddd, *J* = 6.7, 3.9, 1.2 Hz, 1H), 7.56 – 7.28 (m, 10H), 6.98 (d, *J* = 9.4 Hz, 1H), 6.33 – 6.25 (m, 1H), 6.02 (dd, *J* = 9.4, 2.5 Hz, 1H), 5.70 (d, *J* = 7.2 Hz, 1H), 5.45 (d, *J* = 2.7 Hz, 1H), 5.29 (s, 1H), 4.98 (dd, *J* = 9.8, 2.3 Hz, 1H), 4.52 – 4.38 (m, 3H), 4.32 (d, *J* = 8.2 Hz, 1H), 4.21 (d, *J* = 8.2 Hz, 1H), 3.82 (d, *J* = 7.0 Hz, 1H), 2.98 (td, *J* = 6.3, 2.2 Hz, 3H), 2.56 (ddd, *J* = 14.8, 9.5, 6.4 Hz, 1H), 2.49 – 2.32 (m, 4H), 2.31 – 2.17 (m, 3H), 2.04 (t, *J* = 2.7 Hz, 1H), 1.93 (t, *J* = 2.8 Hz, 3H), 1.79 (s, 1H), 1.69 (s, 2H), 1.59 (s, 5H), 1.24 (t, *J* = 2.6 Hz, 4H), 1.14 (s, 2H).

*Synthesis and characterization of compound **21***

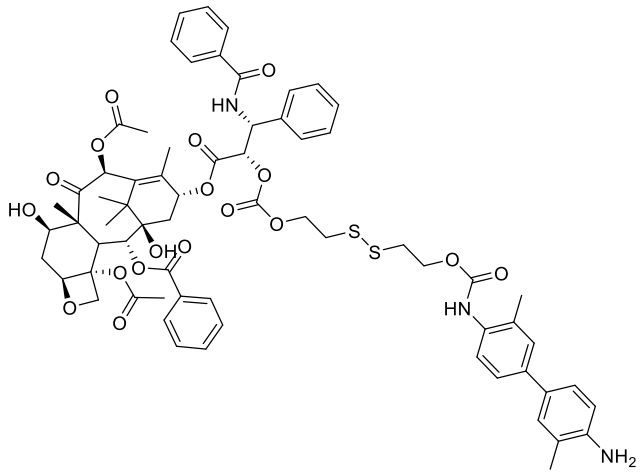

21

Figure 7.20

The reaction was carried out under anhydrous conditions at room temperature for a night. At first hydroxybenzotriazole (HOBt 5.75 mg, 0.042 mmol, **1eq**) was dissolved in 150 µL of dry DMF (with MS 4 Å). Then o-tolidine (13.54 mg, 0.064 mmol, **1.5eq**) and compound **20** (51 mg, 0.043 mmol, **1eq**) were added. After a night, the solvent was removed under vacuum and the crude mixture was washed and filtered with EA. The product (figure 7.20) was purified by silica gel flash column chromatography (Cy : EA = 1:2) affording the pure compound in 54% yield.

^{1}H NMR (400 MHz, acetone) δ 8.56 (d, *J* = 9.2 Hz, 1H), 8.18 – 8.11 (m, 2H), 7.93 – 7.86 (m, 2H), 7.72 – 7.21 (m, 14H), 6.74 (d, *J* = 8.2 Hz, 1H), 6.43 (s, 1H), 6.17 (td, *J* = 9.3, 1.6 Hz, 1H), 6.01 (dd, *J* = 9.1, 5.8 Hz, 1H), 5.69 (d, *J* = 7.2 Hz, 1H), 5.56 (d, *J* = 5.9 Hz, 1H), 4.97 (dd, *J* = 9.7, 2.2 Hz, 1H), 4.49 – 4.41 (m, 2H), 4.35 (td, *J* = 6.3, 2.0 Hz, 2H), 4.20 – 4.14 (m, 2H), 3.90 (s, 1H), 3.85 (d, *J* = 7.0 Hz, 1H), 3.55 (d, *J* = 5.9 Hz, 1H), 3.10 – 2.97 (m, 2H), 2.87 (s, 6H), 2.84 – 2.80 (m, 2H), 2.54 – 2.43 (m, 4H), 2.34 (s, 4H), 2.20 (s, 4H), 2.17 (s, 1H), 2.15 (s, 3H), 1.98 (d, *J* = 1.5 Hz, 3H), 1.66 (s, 2H), 1.29 (s, 1H), 1.18 (d, *J* = 2.1 Hz, 3H).

Synthesis and characterization of compound ***22***

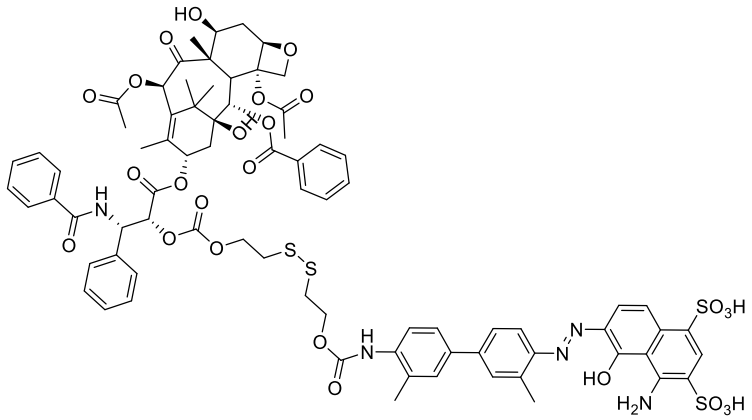

22

Figure 7.21

The diazotation procedure is divided into 3 Steps:

STEP 1

In a vial, compound **21** (29.7 mg, 0.023 mmol) was dissolved in 238 µL of acetonitrile at 0°C. When everything was dissolved, two solutions previously cooled down at 0°C were added, the first one was HCl 0.3 N (238 µL) and after 2 minutes the second one, a solution of $NaNO_2$ (4.76 mg, 0.069 mmol dissolved in 80 µL of MilliQ H_2O), the color change from pink to a cadmium yellow. Then the reaction was left a 0°C for 30 minutes.

STEP 2

In another vial, at 0°C, sodium bicarbonate (6.96 mg, 0.0828 mmol) was dissolved in 274 µL of MilliQ H_2O, subsequently 1-amin-8-naphtol-disulfonic acid was added to this stirred solution.

STEP 3

After the half hour the solution inside the vial of the step 1 was transferred in the solution of the vial of the step 2. The colour changed completely and became violet. Then the reaction was left for 3 hours at 10° C.

To remove water and acetonitrile the mixture was then lyophilized. The crude solid product (figure 7.21) was then dissolved in a little amount of water and MeOH and was put in dialysis to remove the salts that were formed during the diazotation process. This compound was also purified by flash silica gel column (acetone : H_2O = 12:1) with a yield of 67%.

^{1}H NMR (400 MHz, DMSO) δ 9.33 (d, *J* = 8.4 Hz, 1H), 8.98 (s, 1H), 8.48 (s, 1H), 8.34 (s, 1H), 8.09 – 7.82 (m, 7H), 7.77 – 7.36 (m, 18H), 7.18 (dd, *J* = 8.6, 4.2 Hz, 1H), 6.98 (d, *J* = 9.4 Hz, 1H), 6.28 (d, *J* = 4.3 Hz, 1H), 5.83 (d, *J* = 9.3 Hz, 1H), 5.53 (t, *J* = 8.6 Hz, 1H), 5.39 (t, *J* = 8.7 Hz, 2H), 4.91 (t, *J* = 8.7 Hz, 2H), 4.69

(s, 1H), 4.63 (s, 1H), 4.45 – 4.19 (m, 5H), 4.13 – 3.89 (m, 4H), 3.69 (s, 1H), 3.57 (d, *J* = 7.3 Hz, 1H), 3.15 (d, *J* = 3.9 Hz, 1H), 3.08 – 2.89 (m, 5H), 2.69 – 2.61 (m, 1H), 2.38 – 2.22 (m, 8H), 2.20 (s, 1H), 2.08 (q, *J* = 4.8 Hz, 4H), 1.97 (s, 1H), 1.80 (dd, *J* = 18.8, 7.3 Hz, 4H), 1.63 (d, *J* = 13.2 Hz, 2H), 1.48 (s, 5H), 1.38 (s, 1H), 1.25 (d*, J* = 26.1 Hz, 3H), 1.15 (t, *J* = 7.1 Hz, 1H), 1.06 – 0.89 (m, 7H).

Nanoparticles preparation

In a vial, 3.3 mg of the *compound **22*** were dissolved in 1 mL of EtOH. As in the case of compound **17** despite the use of the stirrer and the sonicator the compound was not dissolved and so it was necessary to filtrate the suspension using a paster pipet in which it was inserted a little piece of cotton and a 1 mm layer of silica. After the filtration the solution appear clear and so it was possible to proceed with the nanoprecipitation. After the filtration it was considered a concentration of 3 mg/mL. In a vial containing MilliQ H_2O (filtered on 0.45 µm syringe filter) under stirring, 500 µL of the solution in EtOH were inserted dropwise using a syringe in order to have a solution 1.5 mg/mL. The procedure was the same for the formation of the nanoparticles in the case of the dimer of EpiPTX (compound **6**). After some minutes of stirring half of the solution was taken and inserted in a cuvette previously filled with 1 mL of filtered H_2O or with 1 mL of filtered BSA solution (30 mg/mL) in order to have a volume of 1.8 mL and a concentration of 0.75 mg inside the cuvette. After that the analysis was performed by DLS giving the results shown in paragraph 5.5.3.

Acknowledgments

I would like to thank all the research group at the Institute of Organic Synthesis and Photoreactivity of the Italian National Research Council in Bologna, for giving me the opportunity of this internship. In particular, I would like to thank my supervisor, Dott. Greta Varchi, who had the patience to review this thesis work and following me during the internship; Dott. Cecilia Martini who worked with me and supervised all the laboratory activities, especially for her never ending support; Dott. Andrea Guerrini for his continuous stimuli to experiments, and all the other team members that collaborated to this project and supported my pathway: Dott. Claudia Ferroni, Dott. Marco Ballestri, Dott. Elisa Martella and all the guys that have shared with me their experiences in this environment and given me advice for the future career.

I would like to thank Prof. Mariafrancesca Fochi that despite her busy schedule, had always found the time to be present, including reviewing this thesis work and always supporting me in this project.

Sincere thanks to my parents Vito and Margherita, and my siblings that despite all the difficulties encountered, they never lost the hope and helped me in every situation.

Special thanks also to my friends that in these years have helped and sustained me in this course of study.

And last, but not least I would like to thank my uncles Michele and Donatella, and their sons Riccardo e Federico that during this university course they have been a second family for me.

Bibliography

[1] D. de Moulin, *A Short History of Breast Cancer*. Springer Netherlands, 1989. doi: 10.1007/978-94-009-1059-1.

[2] G. H. Sakorafas and M. Safioleas, "Breast cancer surgery: An historical narrative. Part II. 18th and 19th centuries," *European Journal of Cancer Care*, vol. 19, no. 1, pp. 6–29, Jan. 2010, doi: 10.1111/J.1365-2354.2008.01060.X.

[3] E. Vagia, D. Mahalingam, and M. Cristofanilli, "The landscape of targeted therapies in TNBC," *Cancers*, vol. 12, no. 4. 2020. doi: 10.3390/cancers12040916.

[4] V. T. DeVita and E. Chu, "A history of cancer chemotherapy," *Cancer Research*, vol. 68, no. 21. 2008. doi: 10.1158/0008-5472.CAN-07-6611.

[5] T. Baudino, "Targeted Cancer Therapy: The Next Generation of Cancer Treatment," *Current Drug Discovery Technologies*, vol. 12, no. 1, 2015, doi: 10.2174/1570163812666150602144310.

[6] J. Gallego-Jara, G. Lozano-Terol, R. A. Sola-Martínez, M. Cánovas-Díaz, and T. de Diego Puente, "A Compressive Review about Taxol®: History and Future Challenges," *Molecules (Basel, Switzerland)*, vol. 25, no. 24. 2020. doi: 10.3390/molecules25245986.

[7] Z. Meng *et al.*, "Prodrug strategies for paclitaxel," *International Journal of Molecular Sciences*, vol. 17, no. 5. 2016. doi: 10.3390/ijms17050796.

[8] E. Miele, G. P. Spinelli, E. Miele, F. Tomao, and S. Tomao, "Albumin-bound formulation of paclitaxel (Abraxane® ABI-007) in the treatment of breast cancer," *International Journal of Nanomedicine*, vol. 4, no. 1. 2009. doi: 10.2147/ijn.s3061.

[9] Q. Fu, J. Sun, W. Zhang, X. Sui, Z. Yan, and Z. He, "Nanoparticle Albumin - Bound (NAB) Technology is a Promising Method for Anti-Cancer Drug Delivery," *Recent Patents on Anti-Cancer Drug Discovery*, vol. 4, no. 3, 2009, doi: 10.2174/157489209789206869.

[10] F. Xie, E. de Thaye, A. Vermeulen, J. van Bocxlaer, and P. Colin, "A dried blood spot assay for paclitaxel and its metabolites," *Journal of Pharmaceutical and Biomedical Analysis*, vol. 148, pp. 307–315, Jan. 2018, doi: 10.1016/j.jpba.2017.10.007.

[11] S. Ezrahi, A. Aserin, and N. Garti, "Basic principles of drug delivery systems – the case of paclitaxel," *Advances in Colloid and Interface Science*, vol. 263, pp. 95–130, Jan. 2019, doi: 10.1016/J.CIS.2018.11.004.

[12] Y. Zhang and Z. Zhang, "The history and advances in cancer immunotherapy: understanding the characteristics of tumor-infiltrating immune cells and their therapeutic implications," *Cellular and Molecular Immunology*, vol. 17, no. 8. 2020. doi: 10.1038/s41423-020-0488-6.

[13] J. P. Fernández, K. A. Luddy, C. Harmon, and C. O'Farrelly, "Hepatic tumor microenvironments and effects on NK cell phenotype and function," *International Journal of Molecular Sciences*, vol. 20, no. 17. MDPI AG, Sep. 01, 2019. doi: 10.3390/ijms20174131.

[14] J. Delahousse, C. Skarbek, and A. Paci, "Prodrugs as drug delivery system in oncology," *Cancer Chemotherapy and Pharmacology*, vol. 84, no. 5. Springer Verlag, pp. 937–958, Nov. 01, 2019. doi: 10.1007/s00280-019-03906-2.

[15] A. M. Grumezescu, *Multifunctional systems for combined delivery, biosensing and diagnostics*. Elsevier, 2017.

[16] D. Peer, J. M. KarP, S. Hong, oMiD C. faroKHzaD, riMona Margalit, and robert langer, "Nanocarriers as an emerging platform for cancer therapy," 2007. [Online]. Available: www.nature.com/naturenanotechnology

[17] G. K. Such, Y. Yan, A. P. R. Johnston, S. T. Gunawan, and F. Caruso, "Interfacing materials science and biology for drug carrier design," *Advanced Materials*, vol. 27, no. 14. 2015. doi: 10.1002/adma.201405084.

[18] L. Yao, X. Xue, P. Yu, Y. Ni, and F. Chen, "Evans Blue Dye: A Revisit of Its Applications in Biomedicine," *Contrast Media and Molecular Imaging*, vol. 2018. 2018. doi: 10.1155/2018/7628037.

[19] E. N. Hoogenboezem and C. L. Duvall, "Harnessing albumin as a carrier for cancer therapies," *Advanced Drug Delivery Reviews*, vol. 130. Elsevier B.V., pp. 73–89, May 01, 2018. doi: 10.1016/j.addr.2018.07.011.

[20] L. Zhou *et al.*, "Dimerization-induced self-assembly of a redox-responsive prodrug into nanoparticles for improved therapeutic index," *Acta Biomaterialia*, vol. 113, 2020, doi: 10.1016/j.actbio.2020.07.007.

[21] H. Wang, M. Xu, M. Xiong, and J. Cheng, "Reduction-responsive dithiomaleimide-based nanomedicine with high drug loading and FRET-indicated drug release," *Chemical Communications*, vol. 51, no. 23, pp. 4807–4810, Mar. 2015, doi: 10.1039/c5cc00148j.

[22] S. R. Dandepally and A. L. Williams, "Microwave-assisted N-Boc deprotection under mild basic conditions using K3PO4·H2O in MeOH," *Tetrahedron Letters*, vol. 50, no. 9, 2009, doi: 10.1016/j.tetlet.2008.12.074.

[23] R. D. Little, "Protective Groups in Organic Synthesis, 3rd Edition Theodora W. Green (The Rowland Institute for Science) and Peter G. M. Wuts (Pharmacia and Upjohn Company). John Wiley & Sons, Inc., New York, NY. 1999. xxi + 779 pp. 15.5 × 23 cm. $84.95. ISBN 0-471-16019-9.," *Journal of Natural Products*, vol. 62, no. 9, 1999, doi: 10.1021/np9907578.

[24] J. Wang, Y. L. Liang, and J. Qu, "Boiling water-catalyzed neutral and selective N-Boc deprotection," *Chemical Communications*, no. 34, pp. 5144–5146, 2009, doi: 10.1039/b910239f.

[25] S. M. Mallikarjuna, C. Sandeep, and B. Padmashali, “Acid Amine Coupling of (1H-Indole-6-yl)(Piperazin-1-yl) Methanone with Substituted Acid Using HATU Coupling Reagent And Their Antimicrobial And Antioxidant Activity,” *International Journal of Pharmaceutical Sciences and Research*, vol. 8, no. 7, 2017.

[26] F. Zhang *et al.*, “Transformative Nanomedicine of an Amphiphilic Camptothecin Prodrug for Long Circulation and High Tumor Uptake in Cancer Therapy,” *ACS Nano*, vol. 11, no. 9, 2017, doi: 10.1021/acsnano.7b03003.

[27] A. Guerrini *et al.*, “A new avenue toward androgen receptor pan-antagonists: C2 sterically hindered substitution of hydroxy-propanamides,” *Journal of Medicinal Chemistry*, vol. 57, no. 17, 2014, doi: 10.1021/jm5005122.

[28] A. Warnecke and F. Kratz, “2,4-Bis(hydroxymethyl)aniline as a building block for oligomers with self-eliminating and multiple release properties,” *Journal of Organic Chemistry*, vol. 73, no. 4, 2008, doi: 10.1021/jo702484z.

[29] Z. L. Li, L. Sun, J. Ma, Z. Zeng, and H. Jiang, “Synthesis and post-polymerization modification of polynorbornene bearing dibromomaleimide side groups,” *Polymer*, vol. 84, pp. 336–342, Feb. 2016, doi: 10.1016/J.POLYMER.2016.01.020.

[30] H. Wang, M. Xu, M. Xiong, and J. Cheng, “Reduction-responsive dithiomaleimide-based nanomedicine with high drug loading and FRET-indicated drug release,” *Chemical Communications*, vol. 51, no. 23, 2015, doi: 10.1039/c5cc00148j.